

RESEARCH



# A shape derivative algorithm for reconstructing elastic dislocations in geophysics

Andrea Aspri<sup>1</sup>, Elena Beretta<sup>2</sup>, Arum Lee<sup>3</sup> and Anna L. Mazzucato<sup>3\*</sup> 

\*Correspondence:  
alm24@psu.edu

<sup>3</sup>Mathematics Department, Penn  
State University, 107 McAllister  
Building, University Park, PA  
16802, USA

Full list of author information is  
available at the end of the article

## Abstract

We consider the inverse problem of determining an elastic dislocation that models a seismic fault in the quasi-static regime of aseismic, creeping faults, from displacement measurements made at the surface of Earth. We derive both a distributed and a boundary shape derivative that encodes the change in a misfit functional between the measured and the computed surface displacement under infinitesimal movements of the dislocation and infinitesimal changes in the slip vector, which gives the displacement jump across the dislocation. We employ the shape derivative in an iterative reconstruction algorithm. We present some numerical test of the reconstruction algorithm in a simplified 2D setting.

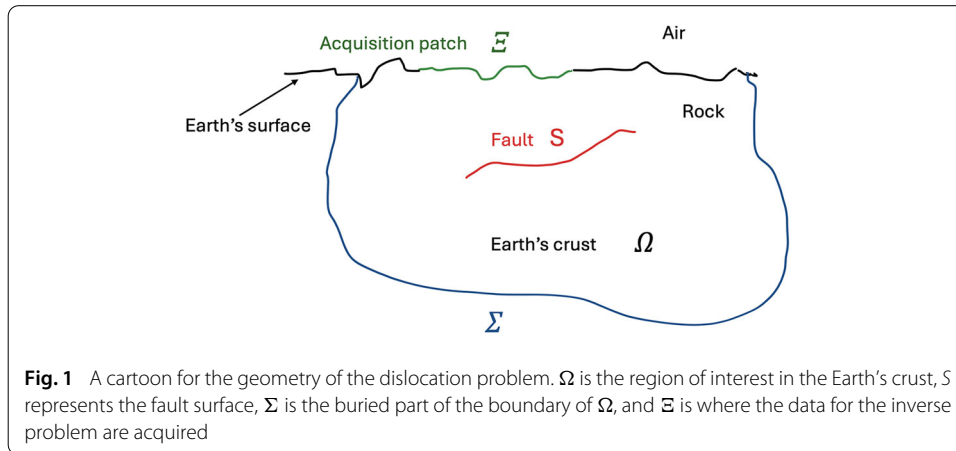
**Keywords:** Elastic dislocation, Slip, Inverse problem, Shape derivative, Iterative reconstruction, Elastostatics, Discontinuous Galerkin, Seismic fault

**Mathematics Subject Classification:** 35R30, 74G75, 65N30

## 1 Introduction

This work concerns an inverse problem for elastic dislocations that model seismic faults. Specifically, we study an iterative reconstruction algorithm for the location and geometry of the fault and the slippage of the rock along the fault. Our algorithm is based on a shape derivative that encodes the changes of a least-square misfit functional between the measured data and a computed solution under infinitesimal deformations of the fault and infinitesimal changes in the slip along the fault.

As customary in seismology, we model the Earth's crust as a linearly elastic medium, but we allow the medium to be inhomogeneous. *We assume throughout that the stiffness parameters in the interior of the Earth are known.* We work locally in a patch in the crust, represented by a bounded domain in  $\mathbb{R}^d$ ,  $d = 2, 3$ , that shares a portion of its boundary with the surface of the Earth. The two-dimensional case is a reduced model that takes into consideration only depth effects in a vertical slice of the crust. The surface of the Earth is clearly not subject to any elastic load, so no elastic forces, that is, no *traction*, can be imposed there, which translates into homogeneous Neumann-type conditions, while there are different physical choices of boundary conditions on the buried part. The fault is



18 modeled as an open surface  $S$  (an open curve in the two-dimensional case) across which  
 19 the elastic displacement jumps, while the normal stress, the traction, remains continuous.  
 20 The jump in the displacement, a vector field  $\mathbf{g}$  on  $S$  called the *slip*, measures how much  
 21 the rock has slipped on each side of the fault surface.

22 The forward or direct problem consists in determining the elastic displacement outside  
 23 of the fault from knowledge of the fault surface and the slip. The inverse problem consists  
 24 in determining the fault surface and the slip from knowledge of the displacement at the  
 25 surface of the Earth. The data are assumed given on an open region of the Earth's surface,  
 26 which we will call the *acquisition manifold*  $\Xi$  (see Fig. 1). The surface displacement can  
 27 be measured from satellite interferometric data or data from global positioning systems  
 28 (GPS). (For a general introduction to the geophysical model we refer to [11,25] and  
 29 references therein.)

30 While the study of elastic dislocations is by now classic, starting with the seminal work  
 31 of Volterra and Somigliana at the turn of the last century (see [34] and the historical  
 32 perspective in [12]), and elastic dislocations have been used to model creeping tectonic  
 33 faults during the interseismic period, especially at subduction zones in the Earth's crust  
 34 (among the vast literature, we mention [15,30,35]), until recently most of the available  
 35 results in the literature dealt with an idealized setting, in which the region of interest in  
 36 the upper layer of the Earth's crust is modeled as an infinite half space (or half plane in  
 37 the two-dimensional case) with constant elasticity parameters, the fault has the simple  
 38 geometry of a rectangle (or segment in the two-dimensional case) with either horizontal or  
 39 oblique orientation, and the slip is constant. In this specialized case then Okada obtained  
 40 an explicit formula for the elastic displacement [22], using the elastic Green's function in  
 41 a half space derived by Mindlin [20].

42 In recent work, it has been observed that the forward problem can be recast as a singu-  
 43 lar source problem or as a nonhomogeneous transmission problem that can be addressed  
 44 using variational techniques or potential theory depending on the regularity of the coef-  
 45 ficients, of the data, and of the domain, including the fault. This has led to establishing  
 46 well-posedness under rather general assumptions on the elastic parameters, the geometry  
 47 of the fault, and the slip [4,6,28,29,31].

48 The inverse problem consists of determining uniquely and then reconstructing the fault  
 49 surface and the slip from boundary measurements. Here, we consider measurements of

50 the elastic displacement made on an open patch of the Earth's surface. Uniqueness in  
51 the inverse problem has already been established under certain geometric conditions on  
52 the fault surface and certain conditions on the slip. For an arbitrary slip field of suitable  
53 regularity, essentially the fault surface must then contain at least one corner singularity [6,  
54 31] (see also the recent preprint [10]). When the slip does not vanish at the boundary of the  
55 fault surface, singularities appear in the elastic displacement near such boundary, which  
56 can help in the reconstruction even in the presence of noise. However, these singularities  
57 are nonphysical, as the elastic displacement diverges. If the slip is assumed to vanish at  
58 the boundary of the fault, a physically justifiable assumption, given that typically only a  
59 part of the fault is active at a time, then in fact uniqueness holds under less stringent and  
60 more natural geometric assumptions on the fault [4]. Informally, faults have to be graphs  
61 but can be arbitrarily oriented.

62 We discuss the precise assumptions for both the direct and the inverse problem in more  
63 detail in Sect. 2. There we also review key well-posedness results for the forward problem  
64 and uniqueness results for the inverse problem.

65 In applications, it is paramount to have a reliable, efficient algorithm to actually recon-  
66 struct the fault and the slip from the measurements. Uniqueness for the inverse problem  
67 provides an important first step in any reconstruction and frames it in the context of a rig-  
68 orous analytic result, especially when the inverse problem is unstable as it is often the case.  
69 We comment more on stability issues below. The reconstruction algorithms available in  
70 the literature (we mention in particular the works [16, 17, 32, 33] and references therein)  
71 consider the case of a homogeneous and isotropic, linearly elastic half space, and a planar  
72 fault. In this case as already mentioned, there is a layer potential representation for the  
73 solution with an explicit kernel. In the case of variable coefficients and more general fault  
74 geometries, the layer potential approach is more difficult to use. The approach we take  
75 instead in this work is to minimize a misfit functional that measures the error between the  
76 computed solution and the measurements at the Earth's surface, using a shape derivative.  
77 We recall that, informally, the shape derivative gives the response of the misfit functional  
78 to infinitesimal movements of the fault and changes in the slip.

79 Shape optimization is a well-developed tool for geometric identification and recon-  
80 struction (we refer the reader, for example, to the monograph [26]). There are typically  
81 two forms for the shape derivative, a *distributed* and a *boundary* form. The distributed  
82 derivative contains volume integrals (respectively, area integrals in two dimensions), while  
83 the boundary derivative is written solely in terms of surface integrals (respectively, line  
84 integrals in two dimensions). With an eye toward a numerical implementation using a  
85 Galerkin method, we derive the shape derivative when the forward problem can be solved  
86 within a variational framework, which holds only when the slip vanishes at the boundary in  
87 a suitable sense. The distributed shape derivative is then obtained by solving the forward  
88 problem together with a certain adjoint problem, which can be done efficiently using, for  
89 instance, a finite element method (FEM) or a discontinuous Galerkin (DG) method. By  
90 contrast, because it uses surface integrals, the boundary shape derivative usually requires  
91 more regularity on the solution of the forward and adjoint problems in order to be com-  
92 puted. The minimal regularity of the boundary, the interface, and the data needed to  
93 calculate the shape derivative in both distributed and boundary forms has been carefully  
94 studied, at least for scalar problems. We mention in particular the work [19].

95 The minimization of the misfit functional follows a steepest descent algorithm, which  
96 *we implement only in the two-dimensional setting*. The numerical experiments tend to  
97 be expensive computationally, because *two* boundary-value problems for the system of  
98 elasticity, the forward and the adjoint problem, must be solved at each step of the descent.  
99 Therefore, as a *proof of concept*, we present the numerical results in a simplified setting,  
100 that of a square as the domain  $\Omega$  and where the fault  $S$  is a line segment. Furthermore,  
101 we mostly focus on the reconstruction of the fault surface assuming the slip is known.  
102 Indeed, the inverse problem is linear in the slip vector and hence stable, while the inverse  
103 problem for the fault surface is nonlinear. We then borrow the approach developed in [9]  
104 for reconstructing polygonal partitions in EIT to do the descent.

105 In this approach, the vertices of the dislocation line are assumed to be nodes of a  
106 coarse domain partition and are moved individually using the shape derivative calculated  
107 along linear elements on the partition. The optimal position of each vertex is computed  
108 separately and used to update the dislocation segment. The advantage of this method  
109 is that it is local to each node of the partition; hence, it can be parallelized to increase  
110 efficiency. The drawback is its accuracy. To calculate the shape derivative, we employ a  
111 DG method to compute both the forward and the adjoint problem on a finer conforming  
112 mesh. The steepest descent algorithm is stopped when a given tolerance is reached. As  
113 with most iterative methods, we have a good reconstruction only if the initial guess is  
114 sufficiently close to the true data for the problem (the fault surface and the slip vector).  
115 Moreover, the limited accuracy of our approach, the inherent sensitivity of the shape  
116 derivative to small changes, and the underlying ill-posedness of the inverse problem make  
117 the reconstruction algorithm numerically less stable. Even though we rigorously derive the  
118 shape derivative only when the slip vanishes at the boundary, the discretized numerical  
119 algorithm can be applied in more generality (see also Remark 2.4). In our numerical  
120 experiments, as expected, we find that if the slip vector is constant, hence singularities  
121 appear in the solution at the tips of the dislocation segment, the reconstruction is more  
122 accurate, since the singularities help in locating the fault boundary. On the other hand,  
123 the error is significantly larger if the slip vector is allowed to vanish at the endpoints (see  
124 [7] where a reconstruction algorithm for linear cracks in dimension two is presented and  
125 tested). Consequently, in this latter situation we find that we may have to make more than  
126 one measurement or measure on a sufficiently large portion of the boundary, while from  
127 the uniqueness result for the inverse problem one would expect that one measurement  
128 on a small open patch at the boundary should be enough to reconstruct.

129 We do not address the stability of the reconstruction, nor the convergence of the method  
130 analytically, issues that we reserve to address in future work. In the case of planar faults  
131 and homogeneous elastic parameters, Lipschitz stability for the inverse fault problem was  
132 proved in [27], albeit leading to a nonquantitative estimate, which therefore cannot be  
133 directly employed to establish convergence. Quantitative Lipschitz stability estimates for  
134 a linear crack were obtained in dimension 2 in [8].

135 We close the Introduction with a brief overview of the paper. In Sect. 2, we discuss the  
136 set up for both the forward and the inverse problem and recall the well-posedness results  
137 for the forward problem, as well as the uniqueness results for the inverse problem in [4,6].  
138 Section 3 is devoted to the rigorous derivation of the shape derivative. Lastly, in Sect. 4,  
139 we discuss the numerical tests and their outcomes.

## 140 2 Preliminaries

141 We start by discussing the set-up for the forward problem and the assumptions we make  
142 on the fault surface and on the slip vector. We follow the notation and conventions in  
143 [4,6]. We only discuss the three-dimensional case with obvious modification in the two-  
144 dimensional case, which is the setting for our numerical experiments.

145 We start by introducing some notation. We employ the blackboard font, e.g.,  $\mathbb{A}$ , for  
146 tensors, the boldface font, e.g.,  $\mathbf{A}$ , for matrices, bold italics font, e.g.,  $\mathbf{a}$ , for vectors, and  
147 italics font, e.g.,  $a$ , for scalars. We denote matrix–vector multiplication simply by  $\mathbf{A}\mathbf{b}$ , while  
148  $\cdot$  and  $:$  represent the inner product between vectors and matrices, respectively. Lastly, we  
149 use Einstein notation of summation over repeated indices, e.g.,  $\mathbf{c}^i = [\mathbf{A}\mathbf{b}]^i = \mathbf{A}^{ij}\mathbf{b}_j$ ; and  
150 we similarly define the product of a tensor with a vector  $\mathbb{A}\mathbf{a}$ .

151 As in [4], we are concerned with faults buried in the Earth’s crust that undergo a creeping  
152 aseismic movement. Such a situation is typical of areas of microseismicity, but can lead  
153 to earthquakes of sizeable magnitude [14]. In this context, faults tend to be shallow, and  
154 it is reasonable to work in a patch of the Earth’s crust, modeled as a bounded domain  
155  $\Omega$  with Lipschitz boundary. In the numerical implementation,  $\Omega$  is of polygonal type.  
156 The boundary of  $\Omega$ ,  $\partial\Omega$ , is subdivided into two parts, one that represent the buried part  
157  $\Sigma$  and the other,  $\partial\Omega \setminus \Sigma$ , that lies on the surface of the Earth. We assume that  $\Sigma$  is  
158 a closed subset of  $\partial\Omega$ . We model the fault by an open, orientable, Lipschitz surface  $S$ ,  
159 with Lipschitz boundary  $\partial S$  at positive distance  $\delta$  from the boundary of  $\Omega$ . We assume  
160 that  $S$  can be extended to a closed Lipschitz surface  $\Gamma$  also at positive distance from  
161  $\partial\Omega$ . Then  $\Gamma$  splits  $\Omega$  into two (possibly disconnected) components  $\Omega^+$  and  $\Omega^-$ , with  
162  $\partial\Omega^- = \Gamma$ ,  $\partial\Omega \cap \partial\Omega^- = \emptyset$  and  $\Omega^+ = \Omega \setminus \overline{\Omega^-}$ . We denote with  $\mathbf{n}$  the unit outer norm to  
163  $\partial\Omega$  and the unit outer normal to  $\Omega^-$ , which induces an orientation on  $S$ .

164 We follow standard notation for function spaces—for instance,  $W^{s,p}(\Omega)$ ,  $s \geq 0$ ,  $1 \leq p \leq$   
165  $\infty$ , denotes  $L^p$ -based Sobolev spaces and  $W^{s,2}(\Omega) = H^s(\Omega)$ . The space  $H_0^{1/2}(\Omega)$  denotes,  
166 as customary, the closure of  $C_c^\infty(\Omega)$  in the  $H^s$  norm. We also define Sobolev spaces  $H^s(\partial\Omega)$   
167 on the boundary of  $\Omega$  and  $H^s(S)$  on the fault  $S$  for  $0 \leq s < 1$ , using partitions of unity  
168 and a flattening of the boundary, which is justified by the regularity assumptions we have  
169 made on  $\Omega$  and  $S$ . Additionally, we introduce Sobolev spaces of vector fields with zero  
170 trace on  $\Sigma$ . If  $V$  is an open subset of  $\Omega$  with Lipschitz boundary and  $\Sigma \subset \partial V$ , we set:

$$171 \quad H_\Sigma^s(V) := \{\mathbf{u} \in H^s(V), \mathbf{u}|_\Sigma = \mathbf{0}\}, \quad s > \frac{1}{2}. \quad (2.1)$$

172 We will also employ a less standard space on  $S$ , the space  $H_{00}^{\frac{1}{2}}(S)$ , which can be defined  
173 as the weighted space:

$$174 \quad H_{00}^{\frac{1}{2}}(S) := \left\{ \mathbf{u} \in H_0^{\frac{1}{2}}(S), \delta^{-1/2}\mathbf{u} \in L^2(S) \right\}, \quad (2.2)$$

175 where  $\delta(x) = \text{dist}(x, \partial S)$  for  $x \in S$  and the distance is computed using geodesic length on  
176  $S$ . The space  $H_{00}^{\frac{1}{2}}$  has the property that if  $S$  is seen as an open patch of a closed Lipschitz  
177 surface  $\Gamma$ , then extension by zero to  $\Gamma$  is a bounded operator from  $H_{00}^{\frac{1}{2}}(S)$  to  $H^{\frac{1}{2}}(\Gamma)$ .  
178 Moreover, elements of  $H_{00}^{\frac{1}{2}}(S)$  have trace zero on  $\partial S$ . We refer to [4, Sect. 2] for further  
179 discussion on this point.

180 Finally, if  $f$  defined a.e. on  $\Omega$  is regular enough to have a nontangential limit on  $S$ , we  
181 let  $[f]_S$  denote the jump on  $S$ , defined as:

$$182 \quad [f]_S = f_+ - f_-,$$

183 where  $f_{\pm}$  is the limit taken nontangentially in  $\Omega^{\pm}$ , respectively.

184 In the regime of creeping faults, where notable slip occurs without earthquakes, a quasi-  
 185 static approximation is justified. Therefore, we model the Earth’s crust as a linearly elas-  
 186 tic, but inhomogeneous, material with time-independent elastic parameters. The elastic  
 187 response is encoded in a fourth-order tensor  $\mathbb{C}$ , the elasticity tensor, which we assume  
 188 to be totally symmetric (that is, the material is hyperelastic) and uniformly Lipschitz  
 189 continuous in  $\Omega$ :

$$190 \quad \mathbb{C} \in W^{1,\infty}(\Omega). \tag{2.3}$$

191 In fact, we assume that  $\mathbb{C}$  is isotropic for the inverse problem. This regularity assumption  
 192 is not optimal in the context of geophysical applications, since the Earth’s crust is typically  
 193 modeled as a layered medium, where material properties can vary abruptly from one layer  
 194 to the next. However, Lipschitz regularity is needed to compute the shape derivative, and  
 195 for the solvability of the forward problem in some cases as well. We discuss this point  
 196 further later in this section.

197 We also impose the standard (uniform) strong convexity condition, which reads

$$198 \quad \mathbb{C}(\mathbf{x})\mathbf{A} : \mathbf{A} \geq \gamma |\mathbf{A}|^2, \quad \text{a.e in } \Omega, \tag{2.4}$$

199 for all symmetric matrices  $\mathbf{A}$  for some constant  $\gamma > 0$ . This condition guarantees that the  
 200 energy functional is strictly positive.

201 The forward or direct fault problem consists in finding the elastic displacement  $\mathbf{u}$  that  
 202 solves the homogeneous elastostatics system subject to suitable boundary conditions on  
 203  $\partial\Omega$  and suitable transmission conditions on  $S$ . On the part of  $\partial\Omega$  that lies on the surface  
 204 of the Earth  $\partial\Omega \setminus \Sigma$ , it is appropriate to assume that there is no elastic load; hence,  $\partial\Omega \setminus \Sigma$   
 205 is traction free. The traction is the normal component of the stress  $\sigma = \mathbb{C}\widehat{\nabla}\mathbf{u}$ , with  $\widehat{\nabla}$  the  
 206 symmetric part of the gradient, and represents the elastic force acting on surfaces.

207 On the buried part  $\Sigma$ , there are several boundary conditions that can be imposed.  
 208 For simplicity, we choose to impose homogeneous Dirichlet conditions, that is,  $\Sigma$  is  
 209 displacement free. This choice is physically motivated by our assumption that the fault is  
 210 at a positive distance from the boundary, so the boundary is undisturbed by the slip on the  
 211 fault. For numerical purposes, absorbing boundary conditions could also be considered.

212 On the fault surface  $S$ , we assume continuity of the traction, while there is a jump in the  
 213 displacement, encoding the slippage of the rock on the two sides of the fault, given by a  
 214 vector field  $\mathbf{g}$  on  $S$ , the so-called *Burger’s vector*. The slip needs not be tangential to  $S$  and  
 215 can be oriented arbitrarily.

216 The displacement  $\mathbf{u}$  must, hence, satisfy the following mixed-boundary-value-interface  
 217 problem:

$$218 \quad \begin{cases} \operatorname{div}(\mathbb{C}\widehat{\nabla}\mathbf{u}) = \mathbf{0}, & \text{in } \Omega \setminus \bar{S}, \\ (\mathbb{C}\widehat{\nabla}\mathbf{u})\mathbf{v} = \mathbf{0}, & \text{on } \partial\Omega \setminus \Sigma, \\ \mathbf{u} = \mathbf{0}, & \text{on } \Sigma, \\ [\mathbf{u}]_S = \mathbf{g}, \quad [(\mathbb{C}\widehat{\nabla}\mathbf{u})\mathbf{n}]_S = \mathbf{0}. \end{cases} \tag{2.5}$$

219 The strong convexity condition (2.4) implies strong ellipticity for the elastostatics operator  
 220  $\operatorname{div}\mathbb{C}\widehat{\nabla}$ . Since we are interested in domains of polyhedral type, elliptic regularity does not  
 221 hold in standard Sobolev spaces and, consequently, problem (2.5) must be intended in a  
 222 weak or very weak sense, depending on the regularity of the slip  $\mathbf{g}$ .

223 As a matter of fact, even when  $\Omega$  and  $S$  are smooth, if  $\mathbf{g}$  does not vanish at the boundary  
 224 of  $S$ , i.e., if  $\mathbf{g} \in H^{\frac{1}{2}}(S)$ , but  $\mathbf{g} \notin H^{\frac{1}{2}}_{00}(S)$ , then singularities develop at  $\partial S$  that preclude  
 225 any variational formulation. Instead, owing to the Lipschitz regularity of the elastic coef-  
 226 ficients, provided the boundary  $\partial\Omega$  is smooth enough, a very weak solution to (2.5) can be  
 227 constructed via a duality argument, viewing the mixed-boundary-value interface problem  
 228 as a singular source problem in the whole of  $\Omega$  with source

$$229 \quad \mathbf{f}_S = \operatorname{div}(\mathbb{C}(\mathbf{g} \otimes \mathbf{n})\delta_S),$$

230 where  $\delta_S$  is the unit measure concentrated on  $S$ , so that  $\mathbf{f}_S \in H^{-3/2-\epsilon}$ ,  $\epsilon > 0$ . To use  
 231 duality, one needs to have sufficiently regular solutions of the adjoint problem, which is  
 232 a problem of the same form in our case. This is possible, since regularity holds for the  
 233 system of elastostatics when  $\Omega$  is sufficiently smooth. In particular, if  $\operatorname{div}(\mathbb{C}\widehat{\nabla}\mathbf{v}) = \mathbf{F}$  in  
 234  $\Omega$  and  $\mathbf{F} \in L^2(\Omega)$ , then  $\mathbf{v} \in H^2(\Omega)$ . Furthermore, it can be shown using a layer potential  
 235 representation that the solution is more regular than obtained via duality, namely, it  
 236 belongs to  $H^{1-\epsilon}(\Omega \setminus \bar{S})$  for any  $\epsilon > 0$ . Hence, the homogeneous Dirichlet condition on  $\Sigma$   
 237 holds in trace sense. Somewhat informally, by a very weak solution of problem (2.5) we  
 238 then mean that  $\mathbf{u}$  satisfies

$$239 \quad \int_{\Omega} \mathbf{u} \cdot \operatorname{div}(\mathbb{C}\widehat{\nabla}\mathbf{v})d\mathbf{x} = \langle \operatorname{div}(\mathbb{C}(\mathbf{g} \otimes \mathbf{n})\delta_S), \mathbf{v} \rangle_{(H^{-3/2-\epsilon}(\Omega), H^{3/2+\epsilon}(\Omega))}$$

241 for all  $\mathbf{v} \in \mathcal{D}(\Omega)$ , where as customary  $\mathcal{D}(\Omega)$  is the space of smooth functions that are  
 242 compactly supported in  $\Omega$ , and  $\langle \cdot, \cdot \rangle_{(X', X)}$  denotes the duality pairing between a Banach  
 243 space  $X$  and its dual  $X'$ . In reality, one needs to work with the dual space of a suitable  
 244 subspace of  $H^1_{\Sigma}(\Omega)$ .

245 For a precise definition of very weak solution and more details on the dual formulation of  
 246 problem (2.5), we refer to [6]. There the domain is the lower half-space and weights must  
 247 be imposed to ensure integrability at infinity. However, essentially the same arguments  
 248 apply in bounded domains, without the need of weights, again if the boundary is sufficiently  
 249 regular (e.g., of class  $C^{2,\alpha}$ ,  $\alpha > 0$ ). We recall the following well-posedness results for very  
 250 weak solutions (see [6, Theorem 3.11]).

251 **Theorem 2.1** *Assume that  $\Omega$  is of class  $C^{2,\alpha}$ ,  $\alpha > 0$ . There exists a very weak solution*  
 252  *$\mathbf{u} \in H^{\frac{1}{2}-\epsilon}(\Omega) \cap H^{1-\epsilon}_{\Sigma}(\Omega \setminus \bar{S})$  to problem (2.5) for any  $\mathbf{g} \in H^{\frac{1}{2}}(S)$  and any  $\epsilon > 0$ .*

253 By contrast, when  $\mathbf{g} \in H^{\frac{1}{2}}_{00}(S)$ , extending the slip by zero to  $\Gamma$  yields a standard non-  
 254 homogeneous interface problem that admits a variational solution in  $H^1(\Omega \setminus \bar{S})$ . The  
 255 variational formulation only requires the elastic parameters to be bounded uniformly.  
 256 We now recall this variational or weak formulation, which will be the starting point for  
 257 computing the shape derivative. Below,  $\tilde{\mathbf{g}} \in H^{\frac{1}{2}}(\Gamma)$  denotes the extension of  $\mathbf{g} \in H^{\frac{1}{2}}_{00}(S)$   
 258 by zero. We recall the following standard lemma (see e.g., [4], Lemma 3.3, and references  
 259 therein).

260 **Lemma 2.2** *The following identification holds:*

$$261 \quad H^1(\Omega \setminus \bar{S}) \cong \tilde{H} := \left\{ f \in L^2(\Omega) : f|_{\Omega^+} \in H^1(\Omega^+), f|_{\Omega^-} \in H^1(\Omega^-), \text{ and } [f]_{\Gamma \setminus \bar{S}} = 0 \right\}. \tag{2.6}$$

263 Then,  $\mathbf{u} \in H^1_\Sigma(\Omega \setminus \bar{S})$  is a weak or variational solution of the mixed-boundary-value-  
 264 interface problem (2.5) if, for all  $\mathbf{v} \in H^1_\Sigma(\Omega)$ :

$$265 \quad a_\Gamma(\mathbf{u}, \mathbf{v}) := \int_{\Omega \setminus \Gamma} \mathbb{C} \widehat{\nabla} \mathbf{u} : \widehat{\nabla} \mathbf{v} \, dx = 0, \tag{2.7}$$

266 and  $[\mathbf{u}]_\Gamma = \tilde{\mathbf{g}}$ . We note that by the symmetry properties of  $\mathbb{C}$ , the bilinear form  $a$  defined  
 267 above can be written equivalently as:

$$268 \quad a_\Gamma(\mathbf{u}, \mathbf{v}) = \int_{\Omega \setminus \Gamma} \mathbb{C} \nabla \mathbf{u} : \nabla \mathbf{v} \, dx = \int_{\Omega \setminus \Gamma} \mathbb{C} \nabla \mathbf{v} : \nabla \mathbf{u} \, dx.$$

269 The following well-posedness result holds (see [4, Theorems 3.5 and 3.6]).

270 **Theorem 2.3** *There exists a unique weak solution  $\mathbf{u} \in H^1_\Sigma(\Omega \setminus \bar{S})$  to problem (2.5), which*  
 271 *depends continuously on the slip vector  $\mathbf{g} \in H^{\frac{1}{2}}_0(S)$ .*

272 Very briefly, the proof consists in solving two problems, a mixed Dirichlet–Neumann  
 273 problem in  $\Omega^+$  and a purely Neumann problem in  $\Omega^-$ , with an *unknown* vector potential  
 274  $\boldsymbol{\phi}$  on  $\Gamma$ , which represents the common value of the traction on the two sides of  $\Gamma$ , and  
 275 subsequently solving for  $\boldsymbol{\phi}$  from knowledge of the slip field  $\mathbf{g}$  using a combination of  
 276 Neumann-to-Dirichlet operators for the domains  $\Omega^\pm$ . We refer the reader to [4] for more  
 277 details and the complete proof.

278 *We consider both the case  $\mathbf{g} \in H^{1/2}_0(S)$  and the general case  $\mathbf{g} \in H^{1/2}(S)$  for the numerical*  
 279 *experiments in Sect. 4.*

280 **Remark 2.4** We present a detailed derivation of the shape derivative in the case  $\mathbf{g} \in$   
 281  $H^{\frac{1}{2}}_0(S)$ , that is, when the solution  $\mathbf{u} \in H^1(\Omega \setminus \bar{S})$ , since the variational setting is the  
 282 best suited for numerical applications. Moreover, assuming that  $\mathbf{g}$  vanishes at  $\partial S$  is more  
 283 physically justified (only a patch on a fault is typically active). However, the boundary  
 284 shape derivative can also be obtained using a layer potential representation of the elastic  
 285 displacement  $\mathbf{u}$ , which we established in [6], following the approach used in [8]. This  
 286 derivation applies to any slip field  $\mathbf{g} \in H^{\frac{1}{2}}(S)$ , including the case of constant slip. As  
 287 mentioned in the Introduction, having singularities at the boundary of  $S$  helps with the  
 288 inverse problem of recovering the shape and location of  $S$ .

289 We close this section by recalling two uniqueness results for the inverse problem of  
 290 determining the fault  $S$  and the slip vector  $\mathbf{g}$  from surface measurements of the displace-  
 291 ment  $\mathbf{u}$  on an open subset  $\Xi \subset \partial\Omega \setminus \Sigma$ , henceforth called the *acquisition manifold*. The  
 292 first result is in the setting of Theorem 2.1, while the second is in the setting of Theorem  
 293 2.3. The two results differ in the a priori assumptions imposed on  $S$  and on  $\mathbf{g}$ , which are  
 294 more stringent in the first case.

295 **Theorem 2.5** (Theorem 5.1 in [6]) *Let  $S_1, S_2$  be two piecewise linear fault surfaces that*  
 296 *in addition are graphs with respect to the same coordinate system. Let  $\mathbf{g}_i$  be bounded*  
 297 *tangential fields in  $H^{1/2}(S_i)$  with  $\text{supp } \mathbf{g}_i = \bar{S}_i$ , for  $i = 1, 2$ . Let  $\mathbf{u}_i$ , for  $i = 1, 2$ , be the*  
 298 *unique very weak solution of (2.5) corresponding to  $\mathbf{g} = \mathbf{g}_i$  and  $S = S_i$ . If  $\mathbf{u}_1|_\Xi = \mathbf{u}_2|_\Xi$ ,*  
 299 *then  $S_1 = S_2$  and  $\mathbf{g}_1 = \mathbf{g}_2$ .*

300 The conditions on  $S_i$  and  $\mathbf{g}_i$  in the theorem above can be weakened somewhat.

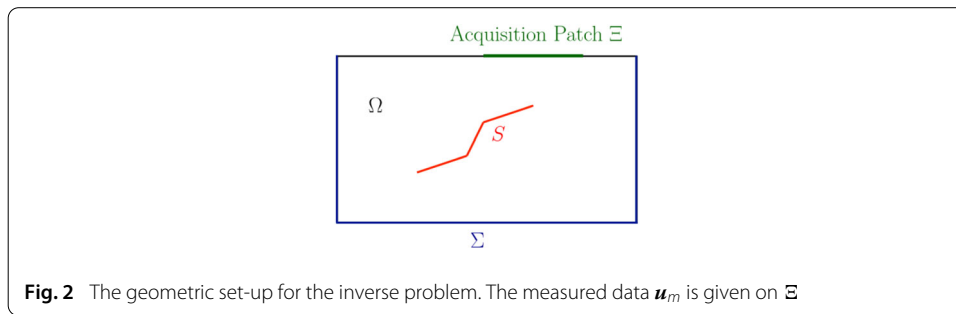


**Fig. 2** The geometric set-up for the inverse problem. The measured data  $\mathbf{u}_m$  is given on  $\Xi$

301 **Theorem 2.6** (Theorem 4.1 in [4]) Let  $S_1, S_2$  be two fault surfaces that in addition are  
 302 graphs with respect to the same coordinate system. Let  $\mathbf{g}_i \in H_{00}^{\frac{1}{2}}(S_i)$ , for  $i = 1, 2$ , with  
 303  $\text{Supp } \mathbf{g}_i = \bar{S}_i$ , for  $i = 1, 2$ , and let  $\mathbf{u}_i$ , for  $i = 1, 2$ , be the unique weak solution of (2.5)  
 304 corresponding to  $\mathbf{g} = \mathbf{g}_i$  and  $S = S_i$ . If  $\mathbf{u}_1|_{\Xi} = \mathbf{u}_2|_{\Xi}$ , then  $S_1 = S_2$  and  $\mathbf{g}_1 = \mathbf{g}_2$ .

305 Briefly, the two theorems above follow both from an argument by contradiction, using  
 306 unique continuation for the elasticity system (this is why we have assumed that  $\mathbb{C}$  is  
 307 Lipschitz continuous and isotropic, but see [5] for certain anisotropic cases). As a matter of  
 308 fact, the boundary condition and the measured data together form the Cauchy data  
 309 on the acquisition manifold  $\Xi$ . Then by unique continuation,  $\mathbf{w} := \mathbf{u}_1 - \mathbf{u}_2$  must be  
 310 identically zero on the connected component of  $\Omega \setminus \overline{S_1 \cup S_2}$  that touches  $\Xi$ . If a.e. every  
 311 point on  $S_1 \cup S_2$  is accessible from this component, the jump conditions immediately give  
 312 a contradiction. If not, then there is a component of  $\Omega \setminus \overline{S_1 \cup S_2}$  that is not accessible from  
 313  $\Xi$ . The jump conditions allow only to conclude that  $\mathbf{w}$  is an infinitesimal rigid motion, and  
 314 then are the geometric conditions imposed on  $S_i$  and the conditions on  $\mathbf{g}_i$ ,  $i = 1, 2$ , that  
 315 imply  $\mathbf{w}$  can only be the trivial motion. Therefore,  $\mathbf{u}_1 \equiv \mathbf{u}_2$  on the entire  $\Omega$ , a contradiction  
 316 in view of nonhomogeneous jumps  $\mathbf{g}_i$  on  $S_i$ . Again, we refer to [4, 6] for complete proofs.

317 We observe that a single measurement on  $\Xi$  is sufficient for the unique determination  
 318 of both the fault and the slip. The assumption that surfaces are graphs with respect to  
 319 a fixed, but arbitrary, coordinate system is not too restrictive in the geophysical context,  
 320 where nearby faults tend to follow the same orientation. For numerical purposes, we are  
 321 interested in polyhedral surfaces and, hence, both uniqueness theorems apply.

### 322 3 The shape derivative

323 In the rest of the paper we present an iterative reconstruction algorithm based on the  
 324 minimization of a suitable misfit functional. For ease of notation, we use  $\lesssim$  to denote  $\leq C$ ,  
 325 where  $C$  is a constant that may depend on the data, i.e., the Lipschitz norm of  $\mathbb{C}$  and the  
 326 strong convexity constant  $\gamma$ , on  $\Omega$ ,  $S$ , and  $\mathbf{g}$ , which are fixed in computing the derivative  
 327 (Fig. 2).

328 Let  $\mathbf{u}_m$  denote the measurement on the acquisition manifold  $\Xi$ . Assuming no mea-  
 329 surement errors,  $\mathbf{u}_m$  agrees with the trace of the solution to the mixed-boundary-value-  
 330 interface problem (2.5) for a certain fault surface  $S_0$  and slip vector  $\mathbf{g}_0$ . We let  $\mathcal{J}$  denote  
 331 the least-squares fitting cost functional:

$$332 \quad \mathcal{J}(S, \mathbf{g}) := \frac{1}{2} \int_{\Xi} |\mathbf{u}_m(\mathbf{x}) - \mathbf{u}(\mathbf{x})|^2 d\sigma(\mathbf{x}), \tag{3.1}$$

333 where  $\mathbf{u}$  solves (2.5) with fault surface  $S$  and slip vector  $\mathbf{g}$  and  $\sigma(\mathbf{x})$  denotes surface area.  
 334 We remark that  $\mathbf{g}$  depends also on  $S$ , so we have slightly abused notation. However,  
 335 since the inverse problem is linear in the slip vector if  $S$  is fixed, the key step consists of  
 336 reconstructing the fault surface  $S$ . Given the uniqueness results for the inverse problem  
 337 and the well-posedness of the forward problem,  $\mathcal{J}$  has a unique global minimum at  $S = S_0$   
 338 and  $\mathbf{g} = \mathbf{g}_0$ .

339 To find this minimum, we propose a steepest descent algorithm based on a shape  
 340 derivative, defined as the derivative of  $\mathcal{J}$  with respect to infinitesimal movements of the  
 341 fault  $S$  and under infinitesimal changes of the slip vector  $\mathbf{g}$ . Due to the ill-posedness of the  
 342 inverse problem, we regularize the algorithm by minimizing only over piecewise polygonal  
 343 or polyhedral faults. We do not study the convergence of this algorithm theoretically, in  
 344 part because we do not know the convexity properties of  $\mathcal{J}$ . Furthermore, there are  
 345 measurement errors and we compute the solution of the forward problem numerically.  
 346 We discuss the influence of these two types of errors in the section on the numerical tests.

347 In this section, we tackle the computation of the shape derivative in terms of a material  
 348 derivative, which gives the change of the solution  $\mathbf{u}$  of (2.5) under infinitesimal changes  
 349 of the fault  $S$  and the slip  $\mathbf{g}$ . We encode the movement of the fault  $S$  in terms of a bi-  
 350 Lipschitz diffeomorphism  $\phi_\tau : \bar{\Omega} \rightarrow \bar{\Omega}$ , depending on a small parameter  $\tau \in [0, 1)$  with  
 351 the following properties:

- 352 (1)  $\phi_0 = I$ , and  $\phi_\tau|_{\partial\Omega} = I$ , where  $I$  is the identity map;
- 353 (2)  $\phi_\tau$  is linear in  $\tau$ .

354 Since  $S$  is at positive distance from  $\partial\Omega$ , there exists  $\delta > 0$  such that  $\text{dist}(\phi_\tau(S), \partial\Omega) > \delta$   
 355 for all  $\tau \in [0, 1)$ . Therefore, we can assume without loss of generality that:

$$356 \quad \phi_\tau := I + \tau \mathcal{U}, \tag{3.2}$$

357 where  $\mathcal{U} : \Omega \rightarrow \Omega$  is a Lipschitz map with support in a neighborhood  $V$  of  $\Gamma$ . (We recall  
 358 that  $\Gamma$  is at positive distance from  $\partial\Omega$ , so  $V$  always exists.) Then:

$$359 \quad \frac{d\phi_\tau}{d\tau} = \mathcal{U}, \quad D_x\phi_\tau = I + \tau D_x\mathcal{U}.$$

360 Similarly, we encode the infinitesimal change of the slip  $\mathbf{g}$  in terms of a vector field  $\mathbf{g}_\tau$ ,  
 361 given by:

$$362 \quad \mathbf{g}_\tau := \mathbf{g} + \tau \mathbf{h}, \tag{3.3}$$

363 where  $\mathbf{h} \in H_{00}^{\frac{1}{2}}(S)$ , and again denote with  $\tilde{\mathbf{g}}_\tau$  its extension by zero to  $\Gamma$ . The actual change  
 364 in the slip is given by the composition of  $\mathbf{g}_\tau$  with  $\phi_\tau^{-1}$ .

365 For notational convenience, we set:

$$366 \quad S_\tau := \phi_\tau(S), \quad \Gamma_\tau := \phi_\tau(\Gamma), \tag{3.4}$$

367 so that  $S_0 \equiv S$  and  $\Gamma_0 \equiv \Gamma$ . We recall that we assume that the elasticity tensor  $\mathbb{C}$  is known  
 368 in both the forward and the inverse problem; it is defined on the whole of  $\bar{\Omega}$  and globally  
 369 Lipschitz continuous.

370 We first obtain a distributed derivative, which can be computed in the framework of  
 371 weak solutions of (2.5), assuming the slip  $\mathbf{g} \in H_{00}^{\frac{1}{2}}(S)$ . We hence work with  $\Gamma_\tau$  and the  
 372 extensions  $\tilde{\mathbf{g}}_\tau, \tilde{\mathbf{h}}$  of the slip vectors  $\mathbf{g}_\tau, \mathbf{h}$  by zero to  $\Gamma_\tau$ .

373 For ease of notation, we write  $\mathcal{J}(\tau) := \mathcal{J}(\Gamma_\tau, \tilde{\mathbf{g}}_\tau)$ . We can now define the *shape deriva-*  
 374 *tive* as the directional derivative:

$$375 \quad D_{(\mathcal{U}, \tilde{\mathbf{h}})} \mathcal{J}(\Gamma_\tau, \tilde{\mathbf{g}}_\tau) := \frac{d\mathcal{J}(\tau)}{d\tau} \Big|_{\tau=0}. \tag{3.5}$$

376 Next, we let  $\mathbf{u}_\tau \in H^1_\Sigma(\Omega \setminus \bar{S}_\tau)$  be the (weak) solution of the perturbed problem, which  
 377 exists and is unique by virtue of Theorem 2.6.:

$$378 \quad \begin{cases} \operatorname{div}(\mathbb{C}\widehat{\nabla}\mathbf{u}_\tau) = \mathbf{0}, & \text{in } \Omega \setminus \Gamma_\tau, \\ (\mathbb{C}\widehat{\nabla}\mathbf{u}_\tau)\mathbf{v} = \mathbf{0}, & \text{on } \partial\Omega \setminus \Sigma, \\ \mathbf{u}_\tau = \mathbf{0}, & \text{on } \Sigma, \\ [\mathbf{u}_\tau]_{\Gamma_\tau} = \tilde{\mathbf{g}}_\tau \circ \phi_\tau^{-1}, \quad [(\mathbb{C}\widehat{\nabla}\mathbf{u}_\tau)\mathbf{n}]_{\Gamma_\tau} = \mathbf{0}, \end{cases} \tag{3.6}$$

379 or equivalently:

$$380 \quad a_{\Gamma_\tau}(\mathbf{u}_\tau, \mathbf{v}) = \int_{\Omega \setminus \Gamma_\tau} \mathbb{C}\nabla_y \mathbf{u}_\tau : \nabla_y \mathbf{v} \, dy = 0, \quad [\mathbf{u}_\tau]_{\Gamma_\tau} = \tilde{\mathbf{g}}_\tau \circ \phi_\tau^{-1},$$

381

382 for every  $\mathbf{v} \in H^1_\Sigma(\Omega)$ , where  $\mathbf{y} = \phi_\tau(\mathbf{x})$ .

383 To compute the material derivative, we transform the perturbed problem (3.6) into a  
 384 problem on the fixed domain  $\Omega \setminus \bar{S}$ . We then let

$$385 \quad \check{\mathbf{u}}_\tau(\mathbf{x}) := \mathbf{u}_\tau \circ \phi_\tau(\mathbf{x}), \quad \mathbf{x} \in \Omega \setminus \bar{S}.$$

386 By the change of variable formula, which holds in Lipschitz domains,  $\check{\mathbf{u}}_\tau \in H^1_\Sigma(\Omega \setminus \bar{S})$   
 387 satisfies the variational problem:

$$388 \quad \begin{aligned} a_\tau(\check{\mathbf{u}}_\tau, \mathbf{w}) &:= \int_{\Omega \setminus \Gamma_\tau} \mathbb{C}(\nabla(\check{\mathbf{u}}_\tau \circ \phi_\tau^{-1})) : (\nabla(\mathbf{w} \circ \phi_\tau^{-1})) \, dy \\ &= \int_{\Omega \setminus \Gamma} \mathbb{C}_\tau \nabla_x \check{\mathbf{u}}_\tau [D\phi_\tau]^{-1} : \nabla_x \mathbf{w} [D\phi_\tau]^{-1} J(\phi_\tau) \, dx = 0, \end{aligned} \tag{3.7}$$

389

390 where  $J(\phi_\tau) = \det(D_x \Phi_\tau)$  is the Jacobian determinant,  $\mathbf{w}(\mathbf{x}) = \mathbf{v}(\phi_\tau(\mathbf{x}))$ , and

$$391 \quad \mathbb{C}_\tau(\mathbf{x}) := \mathbb{C}(\phi_\tau(\mathbf{x})). \tag{3.8}$$

392 Above we have again used the symmetry properties of  $\mathbb{C}$ . Additionally, since  $\phi_\tau$  induces  
 393 an automorphism on  $H^1_\Sigma(\Omega)$ , we have dropped the dependence on  $\tau$  on the test function  
 394  $\mathbf{w}$ . We stress that  $\mathbb{C}_\tau$  has the same symmetries and satisfies the same strong convexity  
 395 condition, since they both hold pointwise uniformly in  $\Omega$ , but it is no longer an elasticity  
 396 tensor.

397 It will be convenient to switch to a weak formulation with homogeneous transmission  
 398 conditions, so as to have the same function space for solutions and test functions. To this  
 399 end, we introduce a lift of the slip vector on  $\Gamma$  using a Newtonian potential. Given any  
 400 vector field  $\mathbf{a} \in H^{\frac{1}{2}}(\Gamma)$ , we define its lift  $\ell_a \in H^1(\Omega \setminus \Gamma)$  as any solution to the problem:

$$401 \quad \begin{cases} \Delta \ell_a = 0 \text{ in } \Omega \setminus \Gamma, \\ [\ell_a]_\Gamma = \mathbf{a}, \quad [\partial_n \ell_a]_\Gamma = \mathbf{0}, \\ \operatorname{Supp} \ell_a \subset \Omega, \end{cases} \tag{3.9}$$

402 with  $\partial_n = \mathbf{n} \cdot \nabla$  the normal derivative. We can specify the lift uniquely by requiring that  
 403  $\ell_a \equiv 0$  on  $\Omega \setminus U$ , where  $U$  is the neighborhood of  $\Gamma$ , for instance. The existence of this  
 404 lift in  $H^1(\Omega \setminus \Gamma)$  can be obtained using a double-layer potential representation for the

405 solution, which is well-known for the Laplacian (alternatively, one can apply the same  
406 techniques used to prove Theorem 2.3). We let:

$$407 \quad \bar{\mathbf{u}}_\tau(\mathbf{x}) := \check{\mathbf{u}}_\tau(\mathbf{x}) - \ell_\tau \tilde{\mathbf{h}}(\mathbf{x}), \quad \mathbf{x} \in \Omega \setminus \Gamma. \quad (3.10)$$

408 Then  $\bar{\mathbf{u}}_\tau \in H^1_\Sigma(\Omega \setminus \bar{S})$  and satisfies:

$$409 \quad a_\tau(\bar{\mathbf{u}}_\tau, \mathbf{w}) = -a_\tau(\ell_\tau \tilde{\mathbf{h}}, \mathbf{w}), \quad [\bar{\mathbf{u}}_\tau]_\Gamma = \tilde{\mathbf{g}}, \quad (3.11)$$

410 since  $[\check{\mathbf{u}}_\tau]_\Gamma = \tilde{\mathbf{g}}_\tau = \tilde{\mathbf{g}} + \tau \tilde{\mathbf{h}}$ . Furthermore:

$$411 \quad [\bar{\mathbf{u}}_\tau - \mathbf{u}]_\Gamma = \tilde{\mathbf{g}} - \tilde{\mathbf{g}} = 0 \Rightarrow \bar{\mathbf{u}}_\tau - \mathbf{u} \in H^1_\Sigma(\Omega).$$

412 We now define the *material derivative*  $\dot{\bar{\mathbf{u}}}$   $\in H^1_\Sigma(\Omega)$  as:

$$413 \quad \dot{\bar{\mathbf{u}}} := \frac{d\bar{\mathbf{u}}_\tau}{d\tau} \Big|_{\tau=0} = \lim_{\tau \rightarrow 0^+} \frac{\bar{\mathbf{u}}_\tau - \mathbf{u}}{\tau}, \quad (3.12)$$

414 where the convergence is strongly in  $H^1_\Sigma(\Omega)$ , if the limit exists.

415 Before tackling the existence of the material derivative, we discuss some useful properties  
416 of  $\mathbb{C}$  and  $\phi_\tau$ . We recall that  $\phi_\tau$  and  $\mathbb{C}$  are uniformly Lipschitz on  $\Omega$ . Since  $\phi_\tau = I + \tau \mathcal{U}$ ,  
417 there exists  $\tau$  small enough, say  $\tau \in [0, \tau_0]$ , for some  $\tau_0 \ll 1$ , such that  $\phi_\tau^{-1} \approx I - \tau \mathcal{U}$  and

$$418 \quad \lim_{\tau \rightarrow 0^+} \frac{D\phi_\tau^{-1} - I}{\tau} = -D\mathcal{U}, \quad \lim_{\tau \rightarrow 0^+} \frac{D\phi_\tau - I}{\tau} = D\mathcal{U}, \quad (3.13)$$

419 in  $L^\infty(\Omega)$ . Similarly,  $J(\phi_\tau) \approx J(\phi_\tau^{-1}) \approx 1$  also for  $\tau \in [0, \tau_0]$ , and a straightforward  
420 calculation shows that

$$421 \quad \lim_{\tau \rightarrow 0^+} \frac{J(\phi_\tau^{-1}) - 1}{\tau} = -\text{div}\mathcal{U}, \quad \lim_{\tau \rightarrow 0^+} \frac{J(\phi_\tau) - 1}{\tau} = \text{div}\mathcal{U}, \quad (3.14)$$

422 also in  $L^\infty(\Omega)$ . Additionally:

$$423 \quad \|\mathbb{C}_\tau\|_{W^{1,\infty}(\Omega)} \lesssim \|\mathcal{U}\|_{W^{1,\infty}(\Omega)} \|\mathbb{C}\|_{W^{1,\infty}(\Omega)},$$

424 and similarly for  $\mathbb{C} \circ \phi_\tau^{-1}$ . For ease of notation, we let

$$425 \quad L := \|\mathcal{U}\|_{W^{1,\infty}(\Omega)}.$$

426 We begin with showing that a weak limit exists. We observe that, since the lift of the  
427 jump on  $\Gamma$  satisfies a linear problem,  $\ell_\tau \tilde{\mathbf{h}} = \tau \ell_\tau \tilde{\mathbf{h}}$ . Consequently,  $\ell_\tau \tilde{\mathbf{h}} = \ell_\tau \tilde{\mathbf{h}}$ .

428 **Lemma 3.1** *Let  $\mathbf{u}$  be the unique weak solution of (2.5) with  $\mathbf{g} \in H^{\frac{1}{2}}(S)$  and let  $\bar{\mathbf{u}}_\tau$  be given  
429 in (3.10). Then  $\frac{\bar{\mathbf{u}}_\tau - \mathbf{u}}{\tau}$  converges weakly in  $H^1_\Sigma(\Omega)$  and strongly in  $L^2(\Omega)$  as  $\tau \rightarrow 0^+$ .*

430 **Remark 3.2** Although convergence will be along subsequences (not relabeled), the whole  
431 sequence will converge as we will show uniqueness of the limit later on.

432 *Proof* By Poincaré’s inequality, it is enough to establish a uniform bound on  $\frac{\|\nabla \bar{\mathbf{u}}_\tau - \nabla \mathbf{u}\|_{L^2(\Omega)}}{\tau}$ .

433 We recall that  $[D\phi_\tau]^{-1} \approx I - \tau D\mathcal{U}$  for  $\tau \in [0, \tau_0]$ , so that

$$434 \quad |\widehat{\nabla} \bar{\mathbf{u}}_\tau(\mathbf{x}) - \widehat{\nabla} \mathbf{u}(\mathbf{x})|^2 \lesssim L^2 \left| (\nabla \bar{\mathbf{u}}_\tau(\mathbf{x}) [\widehat{D}\phi_\tau(\mathbf{x})]^{-1}) - (\nabla \mathbf{u}(\mathbf{x}) [\widehat{D}\phi_\tau(\mathbf{x})]^{-1}) \right|^2.$$

436 Next, using the strong convexity assumption (2.4) and the symmetry of  $\mathbb{C}$ , we have that  
437 for a.e.  $\mathbf{x} \in \Omega$ ,

$$438 \quad \left| (\nabla \bar{\mathbf{u}}_\tau(\mathbf{x}) [\widehat{D}\phi_\tau(\mathbf{x})]^{-1}) - (\nabla \mathbf{u}(\mathbf{x}) [\widehat{D}\phi_\tau(\mathbf{x})]^{-1}) \right|^2 \\ 439 \quad \lesssim C(L, \gamma) \mathbb{C} [\nabla(\bar{\mathbf{u}}_\tau - \mathbf{u})(\mathbf{x}) [D\phi_\tau(\mathbf{x})]^{-1}] : [\nabla(\bar{\mathbf{u}}_\tau - \mathbf{u})(\mathbf{x}) [D\phi_\tau(\mathbf{x})]^{-1}].$$

441 It then follows from Korn’s inequality that

$$\begin{aligned}
 & \frac{1}{\tau^2} \int_{\Omega} |\nabla \bar{\mathbf{u}}_{\tau} - \nabla \mathbf{u}|^2 \, d\mathbf{x} \\
 & \lesssim C(L, \gamma) \int_{\Omega} \frac{1}{\tau^2} \mathbb{C} [\nabla (\bar{\mathbf{u}}_{\tau} - \mathbf{u}) [D\phi_{\tau}]^{-1}] : [\nabla (\bar{\mathbf{u}}_{\tau} - \mathbf{u}) [D\phi_{\tau}]^{-1}] \, d\mathbf{x}.
 \end{aligned} \tag{3.15}$$

445 Next we note that, since  $\frac{\bar{\mathbf{u}}_{\tau} - \mathbf{u}}{\tau} \in H^1_{\Sigma}(\Omega)$ , it can be used as a test function in (2.7) for  $\mathbf{u}$   
 446 and in (3.7) for  $\check{\mathbf{u}}_{\tau}$ . Hence, for  $\tau > 0$

$$\begin{aligned}
 & \frac{1}{\tau} \int_{\Omega \setminus \Gamma} \mathbb{C} \nabla \mathbf{u} : \nabla \left( \frac{\bar{\mathbf{u}}_{\tau} - \mathbf{u}}{\tau} \right) \, d\mathbf{x} = 0 \\
 & \frac{1}{\tau} \int_{\Omega \setminus \Gamma} \mathbb{C}_{\tau} \nabla \check{\mathbf{u}}_{\tau} [D\phi_{\tau}]^{-1} : \left[ \nabla \left( \frac{\bar{\mathbf{u}}_{\tau} - \mathbf{u}}{\tau} \right) [D\phi_{\tau}]^{-1} \right] J(\phi_{\tau}) \, d\mathbf{x} = 0
 \end{aligned} \tag{3.16}$$

450 We then write using the fact that we can integrate  $\bar{\mathbf{u}}_{\tau} - \mathbf{u}$  equivalently on  $\Omega$  or  $\Omega \setminus \Gamma$  or  
 451  $\Omega \setminus \Gamma_{\tau}$ :

$$\begin{aligned}
 & \frac{1}{\tau^2} \int_{\Omega} \mathbb{C} [\nabla (\bar{\mathbf{u}}_{\tau} - \mathbf{u}) [D\phi_{\tau}]^{-1}] : [\nabla (\bar{\mathbf{u}}_{\tau} - \mathbf{u}) [D\phi_{\tau}]^{-1}] \, d\mathbf{x} \\
 & = -\frac{1}{\tau^2} \int_{\Omega \setminus \Gamma} \mathbb{C} [\nabla \mathbf{u} [D\phi_{\tau}]^{-1}] : [\nabla (\bar{\mathbf{u}}_{\tau} - \mathbf{u}) [D\phi_{\tau}]^{-1}] \, d\mathbf{x} \\
 & \quad + \frac{1}{\tau^2} \int_{\Omega \setminus \Gamma} \mathbb{C} [\nabla \bar{\mathbf{u}}_{\tau} [D\phi_{\tau}]^{-1}] : [\nabla (\bar{\mathbf{u}}_{\tau} - \mathbf{u}) [D\phi_{\tau}]^{-1}] \, d\mathbf{x} =: A + B.
 \end{aligned}$$

456 We tackle the terms  $A$  and  $B$  separately, exploiting (3.16). For the first term, we have:

$$\begin{aligned}
 A & = - \int_{\Omega \setminus \Gamma} \mathbb{C} \left[ \nabla \mathbf{u} \left( \frac{[D\phi_{\tau}]^{-1} - I}{\tau} \right) \right] : \left[ \nabla \left( \frac{\bar{\mathbf{u}}_{\tau} - \mathbf{u}}{\tau} \right) \right] \, d\mathbf{x} \\
 & \quad - \int_{\Omega \setminus \Gamma} \mathbb{C} [\nabla \mathbf{u} [D\phi_{\tau}]^{-1}] : \left[ \nabla \left( \frac{\bar{\mathbf{u}}_{\tau} - \mathbf{u}}{\tau} \right) \left( \frac{[D\phi_{\tau}]^{-1} - I}{\tau} \right) \right] \, d\mathbf{x}
 \end{aligned}$$

460 Consequently, uniformly in  $\tau \in [0, \tau_0]$ ,

$$|A| \lesssim C(L, \gamma) \|\mathbf{u}\|_{H^1(\Omega \setminus \bar{\Omega})} \left\| \frac{\nabla (\bar{\mathbf{u}}_{\tau} - \mathbf{u})}{\tau} \right\|_{L^2(\Omega)}. \tag{3.17}$$

462 For the second term, we recall the definition of  $\bar{\mathbf{u}}_{\tau}$  (3.10) to obtain:

$$\begin{aligned}
 B & = \int_{\Omega \setminus \Gamma} \frac{1}{\tau} \mathbb{C} [\nabla \check{\mathbf{u}}_{\tau} [D\phi_{\tau}]^{-1}] : \left[ \nabla \left( \frac{\bar{\mathbf{u}}_{\tau} - \mathbf{u}}{\tau} \right) [D\phi_{\tau}]^{-1} \right] \, d\mathbf{x} \\
 & \quad - \int_{\Omega \setminus \Gamma} \mathbb{C} \left[ \nabla \frac{\ell_{\tau} \tilde{\mathbf{h}}}{\tau} [D\phi_{\tau}]^{-1} \right] : \left[ \nabla \frac{(\bar{\mathbf{u}}_{\tau} - \mathbf{u})}{\tau} [D\phi_{\tau}]^{-1} \right] \, d\mathbf{x} =: B_1 + B_2.
 \end{aligned}$$

466 For the first term on the right, using the second equation in (3.16):

$$\begin{aligned}
 B_1 & = \int_{\Omega \setminus \Gamma} \mathbb{C}_{\tau} \left[ \nabla \check{\mathbf{u}}_{\tau} \frac{([D\phi_{\tau}]^{-1} - I)}{\tau} \right] : \left[ \nabla \frac{(\bar{\mathbf{u}}_{\tau} - \mathbf{u})}{\tau} [D\phi_{\tau}]^{-1} \right] \, d\mathbf{x} \\
 & \quad - \int_{\Omega \setminus \Gamma} \frac{(\mathbb{C}_{\tau} - \mathbb{C})}{\tau} [\nabla \check{\mathbf{u}}_{\tau} [D\phi_{\tau}]^{-1}] : \left[ \nabla \frac{(\bar{\mathbf{u}}_{\tau} - \mathbf{u})(\mathbf{x})}{\tau} [D\phi_{\tau}]^{-1} \right] \, d\mathbf{x} \\
 & \quad + \int_{\Omega \setminus \Gamma} \mathbb{C}_{\tau} [\nabla \check{\mathbf{u}}_{\tau} [D\phi_{\tau}]^{-1}] : \left[ \nabla \frac{(\bar{\mathbf{u}}_{\tau} - \mathbf{u})(\mathbf{x})}{\tau} [D\phi_{\tau}]^{-1}(\mathbf{x}) \right] \frac{(J(\phi) - 1)}{\tau} \, d\mathbf{x}
 \end{aligned}$$

471 Hence, for  $\tau \in [0, \tau_0]$  we have the bound:

$$\begin{aligned}
 472 \quad |B_1| &\lesssim C(L, \gamma) \|\dot{\mathbf{u}}_\tau\|_{H^1(\Omega \setminus \bar{S})} \left\| \frac{\nabla(\bar{\mathbf{u}}_\tau - \mathbf{u})}{\tau} \right\|_{L^2(\Omega)} \\
 473 \quad &\lesssim \tilde{C}(L, \gamma) \|\mathbf{u}_\tau\|_{H^1(\Omega \setminus \bar{S}_\tau)} \left\| \frac{\nabla(\bar{\mathbf{u}}_\tau - \mathbf{u})}{\tau} \right\|_{L^2(\Omega)}. \tag{3.18}
 \end{aligned}$$

474 For the second term on the right, we have similarly

$$475 \quad |B_2| \lesssim C(L, \gamma) \|\ell_{\tilde{\mathbf{h}}}\|_{H^1(\Omega \setminus \bar{S})} \left\| \frac{\nabla(\bar{\mathbf{u}}_\tau - \mathbf{u})}{\tau} \right\|_{L^2(\Omega)}, \tag{3.19}$$

476 using also that by linearity  $\ell_{\tau \tilde{\mathbf{h}}/\tau} = \ell_{\tilde{\mathbf{h}}}$ . From (3.15), (3.17), (3.18), (3.19), we then obtain  
 477 the desired uniform bound:

$$478 \quad \left\| \frac{\nabla(\bar{\mathbf{u}}_\tau - \mathbf{u})}{\tau} \right\|_{L^2(\Omega)}^2 \lesssim C \left( L, \gamma, \|\mathbf{h}\|_{H_0^{\frac{1}{2}}(S)} \right) \left\| \frac{\nabla(\bar{\mathbf{u}}_\tau - \mathbf{u})}{\tau} \right\|_{L^2(\Omega)}, \quad \forall \tau \in [0, \tau_0], \tag{3.20}$$

480 where we have employed also the stability estimates for problems (2.5), (3.6), and (3.9).

481 We hence have that, upon passing to a subsequence,  $\frac{\dot{\mathbf{u}}_\tau - \mathbf{u}}{\tau}$  converges weakly to  
 482 an element  $\mathbf{v} \in H_{\Sigma}^1(\Omega)$ . By Rellich Compactness Theorem, the subsequence converges  
 483 strongly in  $L^2(\Omega)$  (in fact, in  $H^s(\Omega)$  for  $s < 1$ ), and by weak continuity of the derivative:

$$484 \quad \frac{\nabla(\bar{\mathbf{u}}_\tau - \mathbf{u})}{\tau} \rightharpoonup \nabla \mathbf{v},$$

485 in  $L^2(\Omega)$ . □

486 *Remark 3.3* For the validity of (3.20), it is not necessary to have  $\mathbb{C}$  globally Lipschitz in  $\Omega$ .  
 487 It is sufficient that  $\mathbb{C}$  is uniformly Lipschitz in a neighborhood of  $\Gamma$ , which also contains  
 488  $\Gamma_\tau$  for  $\tau$  sufficiently small.

489 We next establish uniqueness of the weak limit and strong convergence, by character-  
 490 izing the material derivative as the solution of a certain variational problem.

491 **Theorem 3.4** *In the hypotheses of Lemma 3.1,  $\frac{\bar{\mathbf{u}}_\tau - \mathbf{u}}{\tau}$  converges as  $\tau \rightarrow 0^+$  strongly to*  
 492  *$\dot{\bar{\mathbf{u}}} \in H_{\Sigma}^1$ , which is the unique solution of the variational problem:*

$$\begin{aligned}
 493 \quad \int_{\Omega} \mathbb{C} \nabla \dot{\bar{\mathbf{u}}} : \nabla \mathbf{w} \, dx &= - \int_{\Omega \setminus \Gamma} \mathbb{B} \nabla \mathbf{u} : \nabla \mathbf{w} \, dx - \int_{\Omega \setminus \Gamma} \mathbb{C} \nabla \mathbf{u} : \nabla \mathbf{w} \operatorname{div} \mathcal{U} \, dx \\
 494 \quad &+ \int_{\Omega \setminus \Gamma} \mathbb{C} \nabla \mathbf{u} : \nabla \mathbf{w} D\mathcal{U} \, dx \\
 495 \quad &+ \int_{\Omega \setminus \Gamma} \mathbb{C} \nabla \mathbf{u} D\mathcal{U} : \nabla \mathbf{w} \, dx - \int_{\Omega \setminus \Gamma} \mathbb{C} \nabla \ell_{\tilde{\mathbf{h}}} : \nabla \mathbf{w} \, dx, \tag{3.21}
 \end{aligned}$$

497 for  $\mathbf{w} \in H_{\Sigma}^1(\Omega)$ , where

$$498 \quad \mathbb{B}^{abcd} := \lim_{\tau \rightarrow 0^+} \frac{\mathbb{C}^{abcd} - \mathbb{C}^{abcd}}{\tau} = \mathcal{U}_e \partial_x^e \mathbb{C}^{abcd}, \tag{3.22}$$

499 in  $L^\infty(\Omega)$ .

501 *Remark 3.5* In general, the 4th-order tensor  $\mathbb{B}$  does not enjoy the same symmetry prop-  
 502 erties as  $\mathbb{C}$ , which reflects the fact that the system of elastostatics is not covariant under  
 503 changes of coordinates.

504 *Proof* We begin by showing that any weak limit of  $\frac{\bar{\mathbf{u}}_\tau - \mathbf{u}}{\tau}$  satisfies (3.21). This fact will  
 505 also ensure its uniqueness.

506 We start by writing  $a_\tau(\frac{\bar{\mathbf{u}}_\tau - \mathbf{u}}{\tau}, \mathbf{w})$  for a generic test function  $\mathbf{w} \in H^1_\Sigma(\Omega)$ . We proceed  
 507 as in the computation of terms  $A$  and  $B$  in the proof of Lemma (3.1), again exploiting the  
 508 weak formulation (3.7) for  $\check{\mathbf{u}}_\tau$ :

$$\begin{aligned}
 509 \quad & - \int_\Omega \mathbb{C}_\tau \left[ \frac{(\nabla \bar{\mathbf{u}}_\tau - \nabla \mathbf{u})}{\tau} [D\phi_\tau]^{-1} \right] : [\nabla \mathbf{w} [D\phi_\tau]^{-1}] J(\phi_\tau) \, dx \\
 510 \quad & = \frac{1}{\tau} \int_{\Omega \setminus \Gamma} \mathbb{C}_\tau [\nabla \mathbf{u} [D\phi_\tau]^{-1}] : [\nabla \mathbf{w} [D\phi_\tau]^{-1}] J(\phi_\tau) \, dx \\
 511 \quad & \quad - \int_{\Omega \setminus \Gamma} \mathbb{C}_\tau \left[ \frac{(\nabla \check{\mathbf{u}}_\tau - \nabla \ell_\tau \tilde{\mathbf{h}})}{\tau} [D\phi_\tau]^{-1} \right] : [\nabla \mathbf{w} [D\phi_\tau]^{-1}] J(\phi_\tau) \, dx = \\
 512 \quad & \frac{1}{\tau} \int_{\Omega \setminus \Gamma} \mathbb{C}_\tau [\nabla \mathbf{u} [D\phi_\tau]^{-1}] : [\nabla \mathbf{w} [D\phi_\tau]^{-1}] J(\phi_\tau) \, dx \\
 513 \quad & \quad + \int_{\Omega \setminus \Gamma} \mathbb{C}_\tau [\ell_\tau \tilde{\mathbf{h}} [D\phi_\tau]^{-1}] : [\nabla \mathbf{w} [D\phi_\tau]^{-1}] J(\phi_\tau) \, dx. \tag{3.23} \\
 514
 \end{aligned}$$

515 For notational convenience, we write the above identity abstractly as:  $G_\tau = E_\tau + F_\tau$ .

516 Our goal is to pass to the limit  $\tau \rightarrow 0^+$  in each term. In all three terms, we will use  
 517 the assumptions on  $\mathbb{C}$  and  $\phi_\tau$ , in particular (3.13) and (3.14). We also recall that the  
 518 composition of two Lipschitz maps is still Lipschitz with constant that can be bounded by  
 519 the product of the two Lipschitz constants, which implies in particular that  $\mathbb{C}_\tau \rightarrow \mathbb{C}$  in  
 520  $W^{1,\infty}(\Omega)$  as  $\tau \rightarrow 0$ . Then,

$$521 \quad \frac{(\mathbb{C}_\tau(\mathbf{x}) - \mathbb{C}(\mathbf{x}))}{\tau} = \frac{\mathbb{C}(\mathbf{x} + \tau \mathcal{U}(\mathbf{x})) - \mathbb{C}(\mathbf{x})}{\tau} \xrightarrow{\tau \rightarrow 0^+} (\mathcal{U}(\mathbf{x}) \cdot \nabla_{\mathbf{x}}) \mathbb{C}(\mathbf{x}),$$

522 a.e.  $\mathbf{x} \in \Omega$  and the limit is in  $L^\infty(\Omega)$ , because both  $\mathcal{U}$  and  $\mathbb{C}$  are Lipschitz.

523 We first investigate the behavior as  $\tau \rightarrow 0^+$  of the integral  $G_\tau$  on the left-  
 524 hand side. By Lemma 3.1 the left-hand side consists of the pairing between an  $L^2$   
 525 weakly convergent (sub)sequence  $\frac{\nabla \bar{\mathbf{u}}_\tau - \nabla \mathbf{u}}{\tau}$  and an  $L^2$  strongly convergent sequence  
 526  $J(\phi_\tau) (\mathbb{C}_\tau \nabla \mathbf{w} [D\phi_\tau]^{-1}) [D\phi_\tau]^{-1}$ . This last expression indicates the action of a 4th-order  
 527 tensor onto a 2nd-order tensor yielding a 2nd-order tensor (up to the scalar factor  $J(\phi_\tau)$ ),  
 528 and strong convergence follows from Hölder’s inequality. Then, by weak-strong conver-  
 529 gence:  
 530

$$\begin{aligned}
 531 \quad & G_\tau = - \int_\Omega \mathbb{C}_\tau \left[ \frac{(\nabla \bar{\mathbf{u}}_\tau - \nabla \mathbf{u})}{\tau} [D\phi_\tau]^{-1} \right] : [\nabla \mathbf{w} [D\phi_\tau]^{-1}] J(\phi_\tau) \, dx \\
 532 \quad & = - \int_\Omega J(\phi_\tau) (\mathbb{C}_\tau \nabla \mathbf{w} [D\phi_\tau]^{-1}) [D\phi_\tau]^{-1} : \frac{(\nabla \bar{\mathbf{u}}_\tau - \nabla \mathbf{u})}{\tau} \, dx \\
 533 \quad & \xrightarrow{\tau \rightarrow 0^+} - \int_\Omega \mathbb{C} \nabla \mathbf{w} : \nabla \dot{\bar{\mathbf{u}}} \, dx = - \int_\Omega \mathbb{C} \nabla \dot{\bar{\mathbf{u}}} : \mathbf{w} \, dx. \tag{3.24} \\
 534
 \end{aligned}$$

535 Next, we tackle the first integral  $E_\tau$  on the right-hand side. We split into three parts, taking  
 536 advantage of the fact that  $\mathbf{u}$  solves (2.7):

$$\begin{aligned}
 537 \quad E_\tau &= \frac{1}{\tau} \int_{\Omega \setminus \Gamma} \mathbb{C}_\tau [\nabla \mathbf{u} [D\phi_\tau]^{-1}] : [\nabla \mathbf{w} [D\phi_\tau]^{-1}] J(\phi_\tau) \, dx \\
 538 \quad &= \int_{\Omega \setminus \Gamma} \frac{(\mathbb{C}_\tau - \mathbb{C})}{\tau} [\nabla \mathbf{u} [D\phi_\tau]^{-1}] : [\nabla \mathbf{w} [D\phi_\tau]^{-1}] J(\phi_\tau) \, dx \\
 539 \quad &\quad + \left\{ \int_{\Omega \setminus \Gamma} \mathbb{C} [\nabla \mathbf{u} [D\phi_\tau]^{-1}] : \left[ \nabla \mathbf{w} \frac{([D\phi_\tau]^{-1} - I)}{\tau} \right] J(\phi_\tau) \, dx \right. \\
 540 \quad &\quad \left. + \int_{\Omega \setminus \Gamma} \mathbb{C} \left[ \nabla \mathbf{u} \frac{([D\phi_\tau]^{-1} - I)}{\tau} \right] : [\nabla \mathbf{w} [D\phi_\tau]^{-1}] J(\phi_\tau) \, dx \right\} \\
 541 \quad &\quad + \int_{\Omega \setminus \Gamma} \mathbb{C} [\nabla \mathbf{u} [D\phi_\tau]^{-1}] : [\nabla \mathbf{w}] \frac{(J(\phi_\tau) - 1)}{\tau} \, dx \\
 542
 \end{aligned}$$

543 Using once again the assumptions on  $\mathbb{C}$  and  $\phi_\tau$ , the regularity of  $\mathbf{u}$  and  $\mathbf{w}$ , and Hölder's  
 544 inequality, we can pass to the limit  $\tau \rightarrow 0^+$  in each term above, as follows:

$$\begin{aligned}
 545 \quad E_\tau &\xrightarrow{\tau \rightarrow 0^+} \int_{\Omega \setminus \Gamma} \mathbb{B} [\nabla \mathbf{u}] : [\nabla \mathbf{w}] \, dx \\
 546 \quad &\quad - \left\{ \int_{\Omega \setminus \Gamma} \mathbb{C} [\nabla \mathbf{u} D\mathcal{U}] : [\nabla \mathbf{w}] \, dx + \int_{\Omega \setminus \Gamma} \mathbb{C} [\nabla \mathbf{u}] : [\nabla \mathbf{w} D\mathcal{U}] \, dx \right\} \\
 547 \quad &\quad + \int_{\Omega \setminus \Gamma} \mathbb{C} [\nabla \mathbf{u}] : [\nabla \mathbf{w}] \operatorname{div} \mathcal{U} \, dx, \tag{3.25} \\
 548
 \end{aligned}$$

549 where we have also employed (3.13)-(3.14) and defined  $\mathbb{B}$  by (3.22). Convergence in the  
 550 last term  $F_\tau$  follows straightforwardly from the convergence of  $\phi_\tau$  to  $I$  and of  $\mathbb{C}_\tau$  to  $\mathbb{C}$  in  
 551  $W^{1,\infty}(\Omega)$ :

$$\begin{aligned}
 552 \quad F_\tau &\xrightarrow{\tau \rightarrow 0^+} \int_{\Omega \setminus \Gamma} \mathbb{C} [\ell_{\tilde{\mathbf{u}}}] : [\nabla \mathbf{w}] \, dx. \tag{3.26} \\
 553
 \end{aligned}$$

554 From (3.24)–(3.26) it follows that any weak limit  $\dot{\tilde{\mathbf{u}}}$  must satisfy (3.21). Then the coercivity  
 555 of the bilinear form  $a_\Gamma$  in  $H^1(\Omega)$  implies the uniqueness of  $\dot{\tilde{\mathbf{u}}}$  in this space. Hence, the  
 556 entire family  $\left\{ \frac{\tilde{\mathbf{u}}_\tau - \mathbf{u}}{\tau} \right\}_{0 < \tau \leq \tau_0}$  converges weakly to  $\dot{\tilde{\mathbf{u}}}$  in  $H^1(\Omega)$

557 We can now show that the convergence is actually strong in  $H^1(\Omega)$ . We first observe  
 558 that, since  $\dot{\tilde{\mathbf{u}}} \in H_\Sigma^1(\Omega)$ , we can equivalently integrate on the right-hand side of (3.21) over  
 559  $\Omega$  or  $\Omega \setminus \Gamma$ , and we can use  $\dot{\tilde{\mathbf{u}}}$  as test function  $\mathbf{w}$ . Hence, we can write (3.21) in compact  
 560 form as:

$$\begin{aligned}
 561 \quad a_\Gamma(\dot{\tilde{\mathbf{u}}}, \dot{\tilde{\mathbf{u}}}) &= - \int_{\Omega \setminus \Gamma} \mathbb{B} (\nabla \mathbf{u}) : (\nabla \dot{\tilde{\mathbf{u}}}) \, dx \\
 562 \quad &\quad - \int_{\Omega \setminus \Gamma} \mathbb{C} \nabla \mathbf{u} \cdot \nabla \dot{\tilde{\mathbf{u}}} \operatorname{div} \mathcal{U} \, dx + \int_{\Omega \setminus \Gamma} \mathbb{C} [\nabla \mathbf{u} D\mathcal{U}] \cdot \nabla \dot{\tilde{\mathbf{u}}} \, dx + \int_{\Omega \setminus \Gamma} \mathbb{C} \nabla \mathbf{u} \cdot [\nabla \dot{\tilde{\mathbf{u}}} D\mathcal{U}] \, dx - a_\Gamma(\ell_{\tilde{\mathbf{u}}}, \dot{\tilde{\mathbf{u}}}), \\
 563
 \end{aligned}$$

564 where  $a_\tau$  is defined below (2.7). Next, similarly to (3.15), by Poincaré’s inequality and the  
 565 strong convexity of  $\mathbb{C}$ , we have the estimate:

$$\begin{aligned}
 & \left\| \frac{\bar{u}_\tau - u}{\tau} - \dot{\bar{u}} \right\|_{H^1(\Omega)}^2 \lesssim \left\| \frac{\nabla \bar{u}_\tau - \nabla u}{\tau} - \nabla \dot{\bar{u}} \right\|_{L^2(\Omega)}^2 \\
 & \lesssim C(L, h) \int_{\Omega} \mathbb{C}_\tau \left[ \left( \frac{\nabla(\bar{u}_\tau - u)}{\tau} - \nabla \dot{\bar{u}} \right) D\phi_\tau^{-1} \right] : \left[ \left( \frac{\nabla(\bar{u}_\tau - u)}{\tau} - \nabla \dot{\bar{u}} \right) D\phi_\tau^{-1} \right] J(\phi_\tau) dx \\
 & = a_\tau \left( \frac{\bar{u}_\tau - u}{\tau} - \dot{\bar{u}}, \frac{\bar{u}_\tau - u}{\tau} - \dot{\bar{u}} \right),
 \end{aligned}$$

570 with  $a_\tau$  as in (3.7).

571 We will show that the right-hand side of the expression above goes to zero as  $\tau \rightarrow 0^+$ .  
 572 To this end, we split it into three parts:

$$a_\tau \left( \frac{\bar{u}_\tau - u}{\tau} - \dot{\bar{u}}, \frac{\bar{u}_\tau - u}{\tau} - \dot{\bar{u}} \right) = a_\tau(\dot{\bar{u}}, \dot{\bar{u}}) - 2a_\tau \left( \frac{\bar{u}_\tau - u}{\tau}, \dot{\bar{u}} \right) + a_\tau \left( \frac{\bar{u}_\tau - u}{\tau}, \frac{\bar{u}_\tau - u}{\tau} \right). \tag{3.27}$$

575 The convergence of  $\mathbb{C}_\tau$  to  $\mathbb{C}$  and of  $\phi_\tau$  to  $I$  in  $W^{1,\infty}(\Omega)$  again implies that

$$a_\tau(v_1, v_2) \xrightarrow{\tau \rightarrow 0^+} a_\Gamma(v_1, v_2), \quad \forall v_i \in H^1(\Omega \setminus \Gamma), \quad i = 1, 2. \tag{3.28}$$

577 From (3.28), we immediately have that

$$a_\tau(\dot{\bar{u}}, \dot{\bar{u}}) \xrightarrow{\tau \rightarrow 0^+} a_\Gamma(\dot{\bar{u}}, \dot{\bar{u}}), \tag{3.29}$$

579 Also, the first part of the proof using  $\dot{\bar{u}}$  as test function  $w$  readily yields:

$$a_\tau \left( \frac{\bar{u}_\tau - u}{\tau}, \dot{\bar{u}} \right) \xrightarrow{\tau \rightarrow 0^+} a_\Gamma(\dot{\bar{u}}, \dot{\bar{u}}). \tag{3.30}$$

581 We cannot directly pass to the limit  $\tau \rightarrow 0^+$  in  $a_\tau \left( \frac{\bar{u}_\tau - u}{\tau}, \frac{\bar{u}_\tau - u}{\tau} \right)$ , because we only  
 582 have weak convergence of the arguments at this point. However, we recall the second  
 583 identity in (3.16), which allows us to rewrite this term as:

$$a_\tau \left( \frac{\bar{u}_\tau - u}{\tau}, \frac{\bar{u}_\tau - u}{\tau} \right) = -a_\tau \left( \ell_{\tilde{h}'} \frac{\bar{u}_\tau - u}{\tau} \right) - a_\tau \left( \frac{u}{\tau}, \frac{\bar{u}_\tau - u}{\tau} \right), \tag{3.31}$$

585 using that  $\frac{\ell_{\tilde{h}}}{\tau} = \frac{\tau \ell_{\tilde{h}}}{\tau} = \ell_{\tilde{h}}$ . Although  $u$  and  $\ell_{\tilde{h}}$  are not test function, as they jump across  
 586  $S$ , the definition of  $a_\tau$  only requires the entries to be in  $H^1(\Omega \setminus \Gamma)$ . Consequently, we can  
 587 pass to the limit  $\tau \rightarrow 0^+$  in the first term on the right by (3.28) to obtain:

$$a_\tau \left( \ell_{\tilde{h}'} \frac{\bar{u}_\tau - u}{\tau} \right) \xrightarrow{\tau \rightarrow 0^+} a_\Gamma(\ell_{\tilde{h}'}, \dot{\bar{u}}). \tag{3.32}$$

589 For the second term on the right, we employ arguments similar to those used in the first  
 590 half of the proof, distributing the factor  $1/\tau$  onto strongly converging terms:

$$\begin{aligned}
 591 \quad a_\tau \left( \frac{\mathbf{u}}{\tau}, \frac{\bar{\mathbf{u}}_\tau - \mathbf{u}}{\tau} \right) &= \int_{\Omega \setminus \Gamma} \mathbb{C}_\tau \left[ \nabla \mathbf{u} \frac{[D\phi_\tau]^{-1}}{\tau} \right] : \left[ \nabla \left( \frac{\bar{\mathbf{u}}_\tau - \mathbf{u}}{\tau} \right) [D\phi_\tau]^{-1} \right] J(\phi_\tau) \, dx \\
 592 \quad &= \int_{\Omega \setminus \Gamma} \frac{(\mathbb{C}_\tau - \mathbb{C})}{\tau} \left[ \nabla \mathbf{u} [D\phi_\tau]^{-1} \right] : \left[ \nabla \left( \frac{\bar{\mathbf{u}}_\tau - \mathbf{u}}{\tau} \right) [D\phi_\tau]^{-1} \right] J(\phi_\tau) \, dx \\
 593 \quad &\quad + \int_{\Omega \setminus \Gamma} \mathbb{C} \left[ \nabla \mathbf{u} \left( \frac{[D\phi_\tau]^{-1} - I}{\tau} \right) \right] : \left[ \nabla \left( \frac{\bar{\mathbf{u}}_\tau - \mathbf{u}}{\tau} \right) [D\phi_\tau]^{-1} \right] J(\phi_\tau) \, dx \\
 594 \quad &\quad + \int_{\Omega \setminus \Gamma} \mathbb{C} [\nabla \mathbf{u}] : \left[ \nabla \left( \frac{\bar{\mathbf{u}}_\tau - \mathbf{u}}{\tau} \right) \left( \frac{[D\phi_\tau]^{-1} - I}{\tau} \right) \right] J(\phi_\tau) \, dx \\
 595 \quad &\quad + \int_{\Omega \setminus \Gamma} \mathbb{C} [\nabla \mathbf{u}] : \left[ \nabla \left( \frac{\bar{\mathbf{u}}_\tau - \mathbf{u}}{\tau} \right) \right] \left( \frac{J(\phi_\tau) - 1}{\tau} \right) \, dx, \\
 596
 \end{aligned}$$

597 where in the last term we have used that  $\mathbf{u}$  solves (2.7). Then, using again the assumptions  
 598 on  $\mathbb{C}$  and  $\phi_\tau$ , (3.13) and (3.14), we can pass to the limit  $\tau \rightarrow 0^+$  in each term on the right,  
 599 since we are pairing the weakly convergent sequence  $\frac{\bar{\mathbf{u}}_\tau - \mathbf{u}}{\tau}$  with a strongly convergent  
 600 sequence, obtaining that

$$\begin{aligned}
 601 \quad a_\tau \left( \frac{\mathbf{u}}{\tau}, \frac{\bar{\mathbf{u}}_\tau - \mathbf{u}}{\tau} \right) &\xrightarrow{\tau \rightarrow 0^+} \int_{\Omega \setminus \Gamma} \mathbb{B} \nabla \mathbf{u} : \nabla \dot{\bar{\mathbf{u}}} \, dx + \int_{\Omega \setminus \Gamma} \mathbb{C} \nabla \mathbf{u} : \nabla \dot{\bar{\mathbf{u}}} \operatorname{div} \mathcal{U} \, dx \\
 602 \quad &\quad - \int_{\Omega \setminus \Gamma} \mathbb{C} \nabla \mathbf{u} : \nabla \dot{\bar{\mathbf{u}}} D\mathcal{U} \, dx \\
 603 \quad &\quad - \int_{\Omega \setminus \Gamma} \mathbb{C} \nabla \mathbf{u} D\mathcal{U} : \nabla \dot{\bar{\mathbf{u}}} \, dx = -a_\Gamma(\dot{\bar{\mathbf{u}}}, \dot{\bar{\mathbf{u}}}) - a_\Gamma(\ell_{\tilde{h}}, \dot{\bar{\mathbf{u}}}), \\
 604 \quad &\hspace{15em} (3.33)
 \end{aligned}$$

605 given that  $\dot{\bar{\mathbf{u}}}$  solves (3.21) for any test function  $\mathbf{w} \in H^1_\Sigma(\Omega)$ . From (3.31), using (3.32) and  
 606 (3.33), we have that

$$607 \quad a_\tau \left( \frac{\bar{\mathbf{u}}_\tau - \mathbf{u}}{\tau}, \frac{\bar{\mathbf{u}}_\tau - \mathbf{u}}{\tau} \right) \xrightarrow{\tau \rightarrow 0^+} -a_\Gamma(\ell_{\tilde{h}}, \dot{\bar{\mathbf{u}}}) + a_\Gamma(\dot{\bar{\mathbf{u}}}, \dot{\bar{\mathbf{u}}}) + a_\Gamma(\ell_{\tilde{h}}, \dot{\bar{\mathbf{u}}}) = a_\Gamma(\dot{\bar{\mathbf{u}}}, \dot{\bar{\mathbf{u}}}). \quad (3.34)$$

608 Finally, by employing (3.29), (3.30), and (3.34) in (3.27), we can conclude that:

$$609 \quad a_\tau \left( \frac{\bar{\mathbf{u}}_\tau - \mathbf{u}}{\tau} - \dot{\bar{\mathbf{u}}}, \frac{\bar{\mathbf{u}}_\tau - \mathbf{u}}{\tau} - \dot{\bar{\mathbf{u}}} \right) \xrightarrow{\tau \rightarrow 0^+} a_\Gamma(\dot{\bar{\mathbf{u}}}, \dot{\bar{\mathbf{u}}}) - 2a_\Gamma(\dot{\bar{\mathbf{u}}}, \dot{\bar{\mathbf{u}}}) + a_\Gamma(\dot{\bar{\mathbf{u}}}, \dot{\bar{\mathbf{u}}}) = 0,$$

610 which in turn implies that

$$611 \quad \frac{\bar{\mathbf{u}}_\tau - \mathbf{u}}{\tau} \xrightarrow{\tau \rightarrow 0^+} \dot{\bar{\mathbf{u}}} \text{ in } H^1_\Sigma(\Omega).$$

612 The proof is now complete. □

613 We recall that  $\dot{\bar{\mathbf{u}}}_\tau = \dot{\bar{\mathbf{u}}}_\tau - \ell_{\tilde{h}} \tilde{h}$  and that  $\frac{\ell_{\tilde{h}} \tilde{h}}{\tau} = \ell_{\tilde{h}}$  is constant in  $\tau$ . Then, from Theorem  
 614 3.4 we straightforwardly obtain an expression for the material derivative

$$615 \quad \dot{\bar{\mathbf{u}}} := \lim_{\tau \rightarrow 0^+} \frac{\dot{\bar{\mathbf{u}}}_\tau - \mathbf{u}}{\tau}, \quad (3.35)$$

616 as solution of a variational problem.

617 **Corollary 3.6** Under the hypotheses of Lemma 3.1,  $\frac{\dot{\mathbf{u}}_\tau - \mathbf{u}}{\tau}$  converges to  $\dot{\mathbf{u}} = \dot{\bar{\mathbf{u}}} + \ell_{\tilde{\mathbf{h}}}$   
 618 strongly in  $H^1_\Sigma(\Omega \setminus \bar{S})$  and  $\dot{\mathbf{u}}$  is the unique variational solution of the problem

$$\begin{aligned}
 619 \quad & \int_{\Omega \setminus \bar{S}} \mathbb{C} \nabla \dot{\mathbf{u}} : \nabla \mathbf{v} \, dx = - \int_{\Omega \setminus \bar{S}} \mathbb{B} \nabla \mathbf{u} : \nabla \mathbf{v} \, dx \\
 620 \quad & - \int_{\Omega \setminus \bar{S}} \mathbb{C} \nabla \mathbf{u} : \nabla \mathbf{v} \operatorname{div} \mathcal{U} \, dx + \int_{\Omega \setminus \bar{S}} \mathbb{C} \nabla \mathbf{u} : \nabla \mathbf{v} D\mathcal{U} \, dx + \int_{\Omega \setminus \bar{S}} \mathbb{C} \nabla \mathbf{u} D\mathcal{U} : \nabla \mathbf{v} \, dx, \\
 621 \quad & \\
 622 \quad & \tag{3.36}
 \end{aligned}$$

623 for all  $\mathbf{v} \in H^1_\Sigma(\Omega)$ , and  $[\dot{\mathbf{u}}]_S = \mathbf{h}$ .

624 Above we have used the stability estimates for the forward problem, which imply the  
 625 trace in  $H^{1/2}(\Gamma)$  is continuous with respect to  $\tau$ . We have also used that

$$626 \quad \left[ \frac{\dot{\mathbf{u}}_\tau - \mathbf{u}}{\tau} \right]_\Gamma = \tilde{\mathbf{h}},$$

627 with  $\tilde{\mathbf{h}} = \mathbf{0}$  on  $\Gamma \setminus \bar{S}$ , and employed Lemma 2.2.

628 Now that we have established the existence of the material derivative and derived a  
 629 formula for it, we will use it to compute the shape derivative, defined in (3.5).

630 **Theorem 3.7** Under the hypotheses of Lemma 3.1, if  $\mathbf{u}$  is the unique weak solution of  
 631 problem (2.5) and  $\tilde{\mathbf{g}}_\tau, S_\tau$  are defined as in (3.3), (3.4), respectively, the shape derivative of  
 632 the functional  $\mathcal{J}$  is given by:

$$\begin{aligned}
 633 \quad & \frac{d}{d\tau} \mathcal{J}(S_\tau, \mathbf{g}_\tau) \Big|_{\tau=0} = - \int_{\Omega \setminus \bar{S}} \mathbb{C} [\nabla \mathbf{u} D\mathcal{U}] : \nabla \mathbf{w} \, dx - \int_{\Omega \setminus \bar{S}} \mathbb{C} \nabla \mathbf{u} : [\nabla \mathbf{w} D\mathcal{U}] \, dx \\
 634 \quad & + \int_{\Omega \setminus \bar{S}} \mathbb{C} \nabla \mathbf{u} : \nabla \mathbf{w} \operatorname{div} \mathcal{U} \, dx + \int_S [\mathbb{C}(\nabla \mathbf{w}) \mathbf{h}] \cdot \mathbf{n} \, d\sigma(\mathbf{x}) - \int_{\Omega \setminus \bar{S}} \mathbb{B} \nabla \mathbf{u} : \nabla \mathbf{w} \, dx, \\
 635 \quad & \tag{3.37}
 \end{aligned}$$

636 where  $\mathbf{w} \in H^1_\Sigma(\Omega)$  is the unique weak solution of the adjoint problem:

$$637 \quad \begin{cases} \operatorname{div}(\mathbb{C} \nabla \mathbf{w}) = \mathbf{0}, & \text{in } \Omega, \\ (\mathbb{C} \nabla \mathbf{w}) \mathbf{v} = (\mathbf{u} - \mathbf{u}_m) \chi_E, & \text{on } \partial \Omega \setminus \Sigma, \\ \mathbf{w} = \mathbf{0}, & \text{on } \Sigma. \end{cases} \tag{3.38}$$

639 **Remark 3.8** Using elementary properties of the trace of a matrix, we can rewrite the  
 640 second integral on the right in (3.37) as

$$641 \quad - \int_{\Omega \setminus \bar{S}} \mathbb{C} [\nabla \mathbf{u} D\mathcal{U}^T] : \nabla \mathbf{w} \, dx,$$

642 where the superscript  $T$  denotes the transpose of a matrix. Hence, (3.37) takes the compact  
 643 form:

$$644 \quad \frac{d}{d\tau} \mathcal{J}(S_\tau, \mathbf{g}_\tau) \Big|_{\tau=0} = \int_{\Omega \setminus \bar{S}} \mathbb{M} [\nabla \mathbf{u}] : \nabla \mathbf{w} \, dx + \int_S (\mathbb{C}[\nabla \mathbf{w}] \mathbf{h}) \cdot \mathbf{n} \, d\sigma(\mathbf{x}), \tag{3.39}$$

645 where the so-called *elastic moment tensor*  $\mathbb{M}$  encodes the distributed effect of the infinitesimal  
 646 movement of the fault.  $\mathbb{M}$  is given in terms of its action on matrices by

$$647 \quad \mathbb{M}[\mathbf{A}] := \mathbb{B}[\mathbf{A}] - \mathbb{C} [\mathbf{A}(D\mathcal{U}^T + D\mathcal{U})] + (\operatorname{div} \mathcal{U}) \mathbb{C}[\mathbf{A}], \tag{3.40}$$

648 for  $\mathbf{A}$  any  $d \times d$  matrix. Note that, in general,  $\mathbb{M}$  does not enjoy the same symmetries as  
 649  $\mathbb{C}$  does, unless  $\mathbb{C}$  is constant.

650 *Proof* Since  $\frac{\dot{\mathbf{u}}_\tau - \mathbf{u}}{\tau}$  converges strongly to  $\dot{\mathbf{u}}$  in  $H^1_\Sigma(\Omega \setminus \bar{S})$  by Corollary 3.6, hence in  $L^2(\partial\Omega)$   
 651 by the Trace Theorem, we can differentiate under the integral sign in the definition of the  
 652 functional  $\mathcal{J}$ :

$$653 \quad \frac{d}{d\tau} \mathcal{J}(S_\tau, \mathbf{g}_\tau) \Big|_{\tau=0} = \int_{\Xi} (\mathbf{u} - \mathbf{u}_m) \cdot \dot{\mathbf{u}} \, d\sigma(\mathbf{x}),$$

654 where we used the definition of the material derivative (3.35).

655 Let now  $\mathbf{w}$  solve the adjoint problem (3.38) (this is a standard variational problem that  
 656 admits a unique weak solution by the Lax-Milgram Theorem, for instance). Then, we can  
 657 equivalently write the expression above on the right as:

$$658 \quad \frac{d}{d\tau} \mathcal{J}(S_\tau, \mathbf{g}_\tau) \Big|_{\tau=0} = \int_{\partial\Omega} [\mathbb{C}(\nabla \mathbf{w}) \mathbf{v}] \cdot \dot{\mathbf{u}} \, d\sigma(\mathbf{x}).$$

659 We recall that we can integrate over  $\Omega \setminus \Gamma$  or  $\Omega \setminus \bar{S}$ , because neither  $\mathbf{u}$  nor  $\mathbf{w}$  jump across  
 660  $\Gamma \setminus \bar{S}$ , and that  $\Gamma$  splits  $\Omega$  into an outer region  $\Omega^+$  that touches  $\partial\Omega$  and an inner core  $\Omega^-$ .  
 661 From (3.38), although  $\dot{\mathbf{u}}$  cannot be used as a test function, integrating first in  $\Omega^+$  and then  
 662 in  $\Omega^-$  gives that

$$663 \quad \int_{\partial\Omega} [\mathbb{C}(\nabla \mathbf{w}) \mathbf{v}] \cdot \dot{\mathbf{u}} \, d\sigma(\mathbf{x}) = - \int_{\Omega^+} \mathbb{C} \nabla \mathbf{w} : \nabla \dot{\mathbf{u}} \, d\mathbf{x} - \int_{\Omega^-} \mathbb{C} \nabla \mathbf{w} : \nabla \dot{\mathbf{u}} \, d\mathbf{x}$$

$$664 \quad \quad \quad + \int_{\Gamma} [\mathbb{C}(\nabla \mathbf{w}) \mathbf{n}] \cdot [\dot{\mathbf{u}}]_{\Gamma} \, d\sigma(\mathbf{x}),$$

665 recalling that by convention  $\mathbf{n}$  is the outer normal to  $\Omega_-$ . But we know that the jump  
 666  $[\dot{\mathbf{u}}]_{\Gamma} = \tilde{\mathbf{h}}$  (so, in fact,  $\dot{\mathbf{u}}$  only jumps across  $S$ ), so that we finally have:

$$667 \quad \frac{d}{d\tau} \mathcal{J}(S_\tau, \mathbf{g}_\tau) \Big|_{\tau=0} = - \int_{\Omega \setminus \bar{S}} \mathbb{C} \nabla \mathbf{w} : \nabla \dot{\mathbf{u}} \, d\mathbf{x} + \int_S [\mathbb{C}(\nabla \mathbf{w}) \mathbf{n}] \cdot \mathbf{h} \, d\sigma(\mathbf{x}),$$

668 where we also used that  $\mathbf{w}$  can be taken as test function for (3.36). □

669 We close this section by deriving a *boundary shape derivative* from the distributed  
 670 shape derivative in case  $\mathbb{C}$  is constant, i.e., the rock is homogeneous in the region of  
 671 interest around the fault. While this formula, which contains only integrals over the  
 672 fault  $S$ , may lead to a less stable numerical implementation, it allows a more transparent  
 673 geometric interpretation. We work with strong solutions of (2.5) and (3.38), assuming  
 674 that  $\partial\Omega$ ,  $S$  and  $\mathbf{g}$ ,  $\mathbf{h}$  are regular enough. By a strong solution  $\mathbf{u}$  of (2.5), we mean that  
 675  $\mathbf{u} \in H^2(\Omega \setminus \bar{S}) \cap H^1_\Sigma(\Omega \setminus \bar{S})$  and that the problem (2.5) is attained at least pointwise a.e.  
 676 Similarly, a strong solution  $\mathbf{w} \in H^2(\Omega) \cap H^1_\Sigma(\Omega)$  solves (3.38) at least pointwise a.e.. From  
 677 standard regularity theory, weak solutions are strong solutions if  $\partial\Omega$  and  $S$  are at least of  
 678 class  $C^{1,\alpha}$ ,  $\alpha > 0$ , and  $\mathbf{g}, \mathbf{h} \in H^s_0(S)$ ,  $s \geq 3/2$ . We only compute the derivative in 2 space  
 679 dimensions to simplify the resulting expression.

680 Our starting point is formula (3.39). We show that we can write  $\mathbb{M}[\nabla \mathbf{u}] : \nabla \mathbf{w}$  as the  
 681 divergence of a certain vector  $\mathbf{b}$ . Since we assume that  $\mathbb{C}$  is constant,  $\mathbb{B} \equiv 0$ . Furthermore,  
 682 since both  $\mathbf{u}$  and  $\mathbf{w}$  satisfy the homogeneous system of elasticity a.e. in  $\Omega \setminus \Gamma$ , it is enough  
 683 to show that:

$$684 \quad \mathbb{M}[\nabla \mathbf{u}] : \nabla \mathbf{w} = -\operatorname{div} \mathbf{b} + ((\mathcal{U} \cdot \nabla) \mathbf{w}) \cdot (\operatorname{div}[\mathbb{C} \nabla \mathbf{u}]) + ((\mathcal{U} \cdot \nabla) \mathbf{u}) \cdot (\operatorname{div}[\mathbb{C} \nabla \mathbf{w}]),$$

686 for a suitable vector field  $\mathbf{b}$ . Next, we exploit some elementary tensor calculus. If  $\mathbf{F}$  is  
 687 a matrix and  $\mathbf{a}$  is a vector, by  $\mathbf{aF}$  we mean vector–matrix multiplication (suppressing  
 688 the transpose for notational ease), that is:  $[\mathbf{aF}]_j = \mathbf{a}_i \mathbf{F}_j^i$ , using Einstein’s summation  
 689 convention. Then, it is easy to see that

$$690 \quad \operatorname{div}(\mathbf{aF}) = \mathbf{a} \cdot \operatorname{div}\mathbf{F} + \nabla \mathbf{a} : \mathbf{F}, \tag{3.41}$$

691 where  $[\operatorname{div}\mathbf{F}]_i = \partial_j \mathbf{F}^{ij} = \operatorname{Tr}(\nabla \mathbf{F})^i$ . We let, following the convention above:

$$692 \quad \mathbf{b} = \mathbf{a}_1 \mathbf{F}_1 + \mathbf{a}_2 \mathbf{F}_2 - a \mathcal{U}, \quad \text{with}$$

$$693 \quad \mathbf{a}_1 = (\mathcal{U} \cdot \nabla) \mathbf{w}, \quad \mathbf{a}_2 = (\mathcal{U} \cdot \nabla) \mathbf{u}, \quad a = \mathbb{C}[\nabla \mathbf{u}] : \nabla \mathbf{w},$$

$$694 \quad \mathbf{F}_1 = \mathbb{C}[\nabla \mathbf{u}], \quad \mathbf{F}_2 = \mathbb{C}[\nabla \mathbf{w}], \tag{3.42}$$

696 where  $a$  is a scalar field and we have identified the map  $\mathcal{U}$  with a vector field. We apply  
 697 (3.41) to  $\mathbf{a}_1 \mathbf{F}_1$ :

$$698 \quad \operatorname{div}(\mathbf{a}_1 \mathbf{F}_1) = ((\mathcal{U} \cdot \nabla) \mathbf{w}) (\operatorname{div}[\mathbb{C}\nabla \mathbf{u}]) + \mathbb{C}[\nabla \mathbf{u}] : \nabla ((\mathcal{U} \cdot \nabla) \mathbf{w}),$$

699 and note that

$$700 \quad [\nabla ((\mathcal{U} \cdot \nabla) \mathbf{w})]_j^i = \partial_j (\mathcal{U}^\ell \partial_\ell \mathbf{w}^i) \Rightarrow$$

$$701 \quad \nabla ((\mathcal{U} \cdot \nabla) \mathbf{w}) = [\nabla \mathbf{w}] D\mathcal{U} + (\mathcal{U} \cdot \nabla) \nabla \mathbf{w}.$$

703 Consequently,

$$704 \quad \operatorname{div}(\mathbf{a}_1 \mathbf{F}_1) = ((\mathcal{U} \cdot \nabla) \mathbf{w}) (\operatorname{div}[\mathbb{C}\nabla \mathbf{u}]) + \mathbb{C}[\nabla \mathbf{u}] : [\nabla \mathbf{w}] D\mathcal{U} + \mathbb{C}[\nabla \mathbf{u}] : [(\mathcal{U} \cdot \nabla) \nabla \mathbf{w}].$$

$$705 \tag{3.43}$$

706 Similarly,

$$707 \quad \operatorname{div}(\mathbf{a}_2 \mathbf{F}_2) = ((\mathcal{U} \cdot \nabla) \mathbf{u}) (\operatorname{div}[\mathbb{C}\nabla \mathbf{w}]) + \mathbb{C}[\nabla \mathbf{w}] : [\nabla \mathbf{u}] D\mathcal{U} + \mathbb{C}[\nabla \mathbf{w}] : [(\mathcal{U} \cdot \nabla) \nabla \mathbf{u}]$$

$$708 \quad = ((\mathcal{U} \cdot \nabla) \mathbf{u}) (\operatorname{div}[\mathbb{C}\nabla \mathbf{w}]) + \mathbb{C}[\nabla \mathbf{u}] D\mathcal{U} : \nabla \mathbf{w} + \mathbb{C}[\nabla \mathbf{w}] : [(\mathcal{U} \cdot \nabla) \nabla \mathbf{u}],$$

$$709 \tag{3.44}$$

711 where in the last identity we have used the symmetry of  $\mathbb{C}$ . We also recall that  $\operatorname{div}(a\mathcal{U}) =$   
 712  $a \operatorname{div}\mathcal{U} + \mathcal{U} \cdot \nabla a$ . Using this formula and (3.43)–(3.44), we can write

$$713 \quad \operatorname{div}(\mathbf{b}) = ((\mathcal{U} \cdot \nabla) \mathbf{w}) (\operatorname{div}[\mathbb{C}\nabla \mathbf{u}]) + ((\mathcal{U} \cdot \nabla) \mathbf{u}) (\operatorname{div}[\mathbb{C}\nabla \mathbf{w}]) + \mathbb{C}[\nabla \mathbf{u}] : [\nabla \mathbf{w}] D\mathcal{U}$$

$$714 \quad + \mathbb{C}[\nabla \mathbf{u}] D\mathcal{U} : [\nabla \mathbf{w}] + \mathbb{C}[\nabla \mathbf{u}] : [(\mathcal{U} \cdot \nabla) \nabla \mathbf{w}] + \mathbb{C}[\nabla \mathbf{w}] : [(\mathcal{U} \cdot \nabla) \nabla \mathbf{u}]$$

$$715 \quad - (\operatorname{div}\mathcal{U}) \mathbb{C}[\nabla \mathbf{u}] : \nabla \mathbf{w} - (\mathcal{U} \cdot \nabla) (\mathbb{C}[\nabla \mathbf{u}] : \nabla \mathbf{w}), \tag{3.45}$$

717 pointwise a.e in  $\Omega \setminus \Gamma$ .

718 Now, since  $\mathbb{C}$  is constant, exploiting again the symmetry of  $\mathbb{C}$ ,

$$719 \quad \mathcal{U}^i \partial_i (\mathbb{C}[\nabla \mathbf{u}] : \nabla \mathbf{w}) = \mathcal{U}^i \mathbb{C}[\nabla \mathbf{u}] : \partial_i \nabla \mathbf{w} + \mathcal{U}^i \mathbb{C}[\partial_i \nabla \mathbf{u}] : \nabla \mathbf{w}$$

$$720 \quad = \mathbb{C}[\nabla \mathbf{u}] : [(\mathcal{U}^i \partial_i) \nabla \mathbf{w}] + \mathbb{C}[\nabla \mathbf{w}] : [(\mathcal{U}^i \partial_i) \nabla \mathbf{u}],$$

721 so the last term in (3.45) cancels other two terms in that expression and we conclude that

$$722 \quad \operatorname{div}(\mathbf{b}) = ((\mathcal{U} \cdot \nabla) \mathbf{w}) (\operatorname{div}[\mathbb{C}\nabla \mathbf{u}]) + ((\mathcal{U} \cdot \nabla) \mathbf{u}) (\operatorname{div}[\mathbb{C}\nabla \mathbf{w}])$$

$$723 \quad + \mathbb{C}[\nabla \mathbf{u}] : [\nabla \mathbf{w}] D\mathcal{U} + \mathbb{C}[\nabla \mathbf{u}] D\mathcal{U} : [\nabla \mathbf{w}] - (\operatorname{div}\mathcal{U}) \mathbb{C}[\nabla \mathbf{u}] : \nabla \mathbf{w}.$$

$$724 \tag{3.46}$$

We can now derive the boundary shape derivative. We introduce some convenient notation. Let  $\{\mathbf{t}, \mathbf{n}\}$  be a curvilinear frame on  $\Gamma$ , hence on  $S$ , with  $\mathbf{n}$  coinciding with the unit outer normal to  $\Omega^-$ . We denote the tangential projection by:

$$\mathbf{F}_{\text{tan}} := \mathbf{F}\mathbf{t}, \quad \mathbf{a}_{\text{tan}} := \mathbf{a} \cdot \mathbf{t},$$

where  $\mathbf{F}$  is a matrix and  $\mathbf{a}$  is a vector, and according to our notation  $\mathbf{F}\mathbf{t}$  denotes matrix–vector multiplication. Similarly, we denote the normal projection by:

$$\mathbf{F}_n := \mathbf{F}\mathbf{n}, \quad \mathbf{a}_n := \mathbf{a} \cdot \mathbf{n}.$$

We also employ the short-hand notation:

$$\partial_{\text{tan}} := \mathbf{t} \cdot \nabla, \quad \partial_n := \mathbf{n} \cdot \nabla.$$

**Theorem 3.9** Assume that  $\Omega \subset \mathbb{R}^2$  and the fault  $S$  is of class  $C^{1,\alpha}$ ,  $\alpha > 0$ , that  $\mathbb{C}$  is constant, and  $\mathbf{g}, \mathbf{h} \in H_0^s(S)$ ,  $s \geq 3/2$ . Then the boundary shape derivative of the functional  $\mathcal{J}$  is given by:

$$\frac{d}{d\tau} \mathcal{J}(S_\tau, \mathbf{g}_\tau)|_{\tau=0} = \int_S [\mathcal{U}_{\text{tan}} (\mathbb{C}[\nabla \mathbf{w}]_n - \mathcal{U}_n (\mathbb{C}[\nabla \mathbf{w}]_{\text{tan}})] \cdot (\partial_{\text{tan}} \mathbf{g}) + (\mathbb{C}[\nabla \mathbf{w}]_n) \cdot \mathbf{h} d\sigma(\mathbf{x}), \tag{3.47}$$

where  $\mathbf{u}$  is a strong solution of (2.5) and  $\mathbf{w}$  is a strong solution of (3.38).

*Proof* Since  $\mathbf{u}$  solves (2.5) and  $\mathbf{w}$  solves (3.38), from (3.46) it follows by integrating by parts in  $\Omega^\pm$  that

$$\begin{aligned} \frac{d}{d\tau} \mathcal{J}(S_\tau, \mathbf{g}_\tau)|_{\tau=0} &= - \int_{\Omega \setminus \Gamma} \text{div} \mathbf{b} d\mathbf{x} + \int_S (\mathbb{C}[\nabla \mathbf{w}]_n) \cdot \mathbf{h} d\sigma(\mathbf{x}) \\ &= \int_\Gamma [\mathbf{b}_n]_\Gamma d\sigma(\mathbf{x}) + \int_S (\mathbb{C}[\nabla \mathbf{w}]_n) \cdot \mathbf{h} d\sigma(\mathbf{x}) \\ &= \int_\Gamma \{[(\mathbb{C}[\nabla \mathbf{u}]_n)]_\Gamma \cdot (\mathcal{U} \cdot \nabla) \mathbf{w} + (\mathbb{C}[\nabla \mathbf{w}]_n) \cdot [(\mathcal{U} \cdot \nabla) \mathbf{u}]_\Gamma \\ &\quad - \mathcal{U}_n [\mathbb{C}[\nabla \mathbf{u}] : \nabla \mathbf{w}]_\Gamma\} d\sigma(\mathbf{x}) + \int_S (\mathbb{C}[\nabla \mathbf{w}]_n) \cdot \mathbf{h} d\mathbf{x}. \end{aligned} \tag{3.48}$$

Above we have used that  $\mathcal{U}, \nabla \mathbf{w}$ , and  $(\mathbb{C}[\nabla \mathbf{w}]_n)$  do not jump across  $\Gamma$ . Indeed,  $\mathcal{U}$  is Lipschitz continuous on the whole  $\Omega$ , while  $\mathbf{w} \in H^2(\Omega)$ , so  $[(\nabla \mathbf{w})_{\text{tan}}]_\Gamma = \mathbf{0}$  since  $\mathbf{w}$  is continuous and  $\Gamma$  is regular. Also, the jump in the traction  $(\mathbb{C}[\nabla \mathbf{w}]_n)$  across  $\Gamma$  is zero from (3.38) integrating by parts in  $\Omega^\pm$ . Then, as in [21], one can conclude from these two facts that  $[(\nabla \mathbf{w})_n]_\Gamma = \mathbf{0}$ ; hence, the whole gradient of  $\mathbf{w}$  does not jump across  $\Gamma$ .

Next, using again the continuity of  $\mathbf{w}$  and its traction across  $\Gamma$ , we note that

$$\begin{aligned} [(\mathcal{U} \cdot \nabla) \mathbf{u}]_\Gamma &= [\nabla \mathbf{u}(\mathbf{n} \otimes \mathbf{n} + \mathbf{t} \otimes \mathbf{t})((\mathcal{U} \cdot \mathbf{n})\mathbf{n} + (\mathcal{U} \cdot \mathbf{t})\mathbf{t})]_\Gamma \\ &= [\partial_n \mathbf{u} \mathcal{U}_n + \partial_{\text{tan}} \mathbf{u} \mathcal{U}_{\text{tan}}]_\Gamma \\ &= [\partial_n \mathbf{u}]_\Gamma \mathcal{U}_n + [\partial_{\text{tan}} \mathbf{u}]_\Gamma \mathcal{U}_{\text{tan}} = [\partial_n \mathbf{u}]_\Gamma \mathcal{U}_n + \partial_{\text{tan}} \tilde{\mathbf{g}} \mathcal{U}_{\text{tan}}. \end{aligned} \tag{3.49}$$

Similarly:

$$\begin{aligned} [\mathbb{C}[\nabla \mathbf{u}] : \nabla \mathbf{w}]_\Gamma &= [\nabla \mathbf{u} : \mathbb{C}[\nabla \mathbf{w}]]_\Gamma = [\nabla \mathbf{u}(\mathbf{n} \otimes \mathbf{n}) : \mathbb{C}[\nabla \mathbf{w}]]_\Gamma + [\nabla \mathbf{u}(\mathbf{t} \otimes \mathbf{t}) : \mathbb{C}[\nabla \mathbf{w}]]_\Gamma \\ &= [(\partial_n \mathbf{u}) \cdot (\mathbb{C}[\nabla \mathbf{w}]_n)]_\Gamma + [\partial_{\text{tan}} \mathbf{u} \cdot (\mathbb{C}[\nabla \mathbf{w}]_{\text{tan}})]_\Gamma \\ &= [\partial_n \mathbf{u}]_\Gamma \cdot (\mathbb{C}[\nabla \mathbf{w}]_n) + [\partial_{\text{tan}} \mathbf{u}]_\Gamma \cdot (\mathbb{C}[\nabla \mathbf{w}]_{\text{tan}}) \\ &= [\partial_n \mathbf{u}]_\Gamma \cdot (\mathbb{C}[\nabla \mathbf{w}]_n) + \partial_{\text{tan}} \tilde{\mathbf{g}} \cdot (\mathbb{C}[\nabla \mathbf{w}]_{\text{tan}}). \end{aligned} \tag{3.50}$$

757 Therefore, using (3.49) and (3.50) in the second and third terms on the right-hand side of  
 758 the last equality in (3.48), we obtain

$$\begin{aligned}
 (\mathbb{C}[\nabla \mathbf{w}])_n \cdot [(\mathcal{U} \cdot \nabla) \mathbf{u}]_\Gamma - \mathcal{U}_n [\mathbb{C}[\nabla \mathbf{u}] : \nabla \mathbf{w}]_\Gamma &= (\mathbb{C}[\nabla \mathbf{w}])_n \cdot [\partial_n \mathbf{u}]_\Gamma \mathcal{U}_n + (\mathbb{C}[\nabla \mathbf{w}])_n \cdot (\partial_{\tan} \tilde{\mathbf{g}}) \mathcal{U}_{\tan} \\
 &\quad - (\mathbb{C}[\nabla \mathbf{w}])_n \cdot [\partial_n \mathbf{u}]_\Gamma \mathcal{U}_n - (\mathbb{C}[\nabla \mathbf{w}])_{\tan} \cdot (\partial_{\tan} \tilde{\mathbf{g}}) \mathcal{U}_n \\
 &= (\mathbb{C}[\nabla \mathbf{w}])_n \cdot (\partial_{\tan} \tilde{\mathbf{g}}) \mathcal{U}_{\tan} - (\mathbb{C}[\nabla \mathbf{w}])_{\tan} \cdot (\partial_{\tan} \tilde{\mathbf{g}}) \mathcal{U}_n.
 \end{aligned}$$

760 Inserting this expression into (3.48) finally gives formula (3.47). □

#### 761 4 Numerical implementation

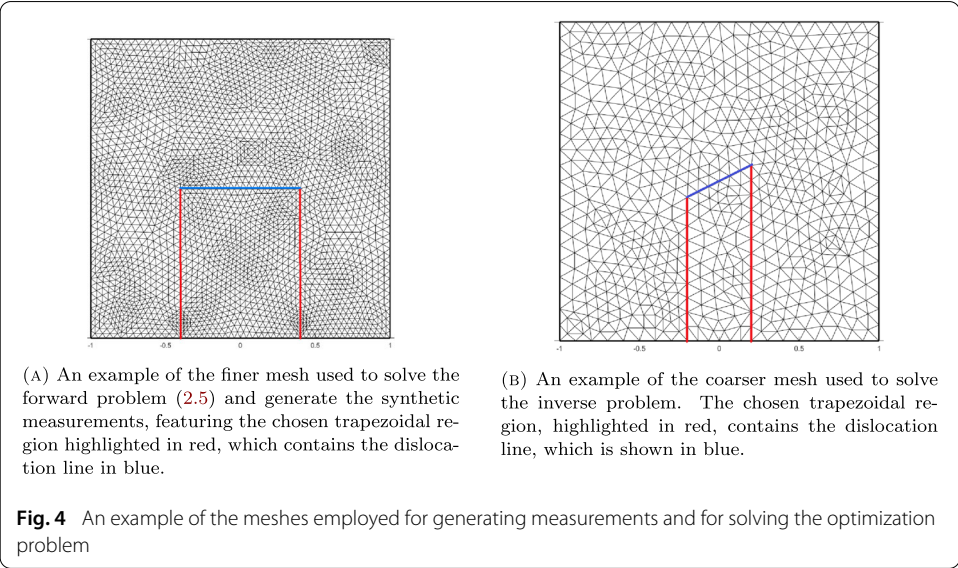
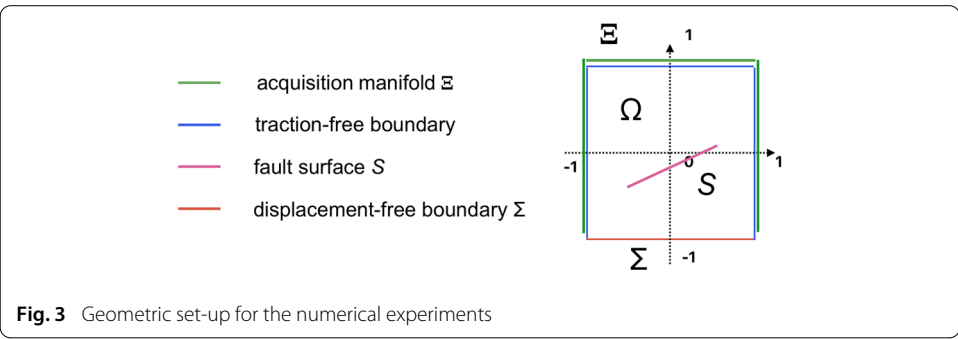
762 In this section, we implement a reconstruction algorithm based on a gradient descent  
 763 method that uses the shape derivative (3.37) of the functional defined in (3.1). While the  
 764 algorithm is applicable in both two and three space dimensions, our numerical experi-  
 765 ments are done in the two-dimensional case, and hence we focus on describing the method  
 766 in 2D. The two-dimensional problem can be seen as looking at vertical slices of the full  
 767 3D problem and neglecting any stress across different slices. This is a simplification, but  
 768 our numerical experiments are a proof of concept that the algorithm can recover the fault  
 769 and the slip under suitable assumptions. We reserve to address a more realistic set-up for  
 770 the numerical implementation in future work.

771 The reconstruction procedure is based on the gradient descent algorithm proposed  
 772 in [9] to reconstruct a piecewise-constant conductivity that jumps across a polygonal  
 773 partition in a composite material from current-to-voltage boundary measurements. There  
 774 are significant differences between the case considered in [9] and here. First of all, we deal  
 775 with a system of PDEs and not a scalar PDE. Furthermore, we have nonhomogeneous  
 776 jumps across the fault. In particular the solution is not  $H^1$  regular across the fault. Lastly,  
 777 we measure only on part of boundary and we measure only once (twice in some unstable  
 778 cases). These additional challenges make the numerical implementation more sensitive,  
 779 especially to how the jump in the displacement  $\mathbf{u}$  across the fault is treated.

780 We concentrate primarily on recovering the fault geometry  $S$ , assuming the slip field  
 781  $\mathbf{g}$  is known. Indeed, once  $S$  is determined, the problem of reconstructing  $\mathbf{g}$  is linear. We  
 782 will consider both situations addressed in our prior works [4, 6], that is, the case when  $\mathbf{g}$   
 783 vanishes at the endpoints of the line  $S$  and is in  $H_{00}^{\frac{1}{2}}(S)$ , and the case that  $\mathbf{g}$  is constant on  
 784  $S$ , even though the theoretical framework for the distributed shape derivative exploits a  
 785 variational formulation and hence applies to the first case.

786 To solve both the forward and adjoint problems (see (2.5) and (3.38)), we employ the  
 787 discontinuous Galerkin (DG) method, which is nonconforming and lends itself to tack-  
 788 ling problems with inhomogeneous jumps. Other numerical methods have been used for  
 789 shape optimization. In the context of elasticity, among the many results we mention the  
 790 recent works [13, 18], where the boundary immerse method and immersed interface finite  
 791 elements are employed.

792 We next discuss the DG method in the context of our problem. For the numerical  
 793 implementation, we let the domain  $\Omega = [-1, 1] \times [-1, 1]$  and  $S$  a segment, positioned  
 794 away from the boundary. Because of the inherent instabilities in the problem, although  
 795 unrealistic for the geophysical problem that motivates our work, we find that we need to  
 796 measure on a sufficiently large part of the boundary. Recall that the acquisition manifold  
 797  $\Xi$  where the measurements are performed lies on the traction-free part of the boundary.  
 798 Hence, we impose homogeneous Neumann conditions on three sides of the square  $\Omega$



799 and homogeneous Dirichlet conditions on the fourth side identified with the set  $\Sigma =$   
 800  $\{(x, y) \mid y = 1, -1 \leq x \leq 1\}$  (See Fig. 3).

801 **4.1 Discontinuous Galerkin (DG) method**

802 We consider a family of shape-regular partitions  $\mathcal{T}_h$  where  $0 < h \ll 1$ . These par-  
 803 titions consist of nonoverlapping triangles  $\mathcal{K}$  such that  $\bar{\Omega} = \cup_{\mathcal{K} \in \mathcal{T}_h} \bar{\mathcal{K}}$ . Specifically,  
 804  $h = \max_{\mathcal{K} \in \mathcal{T}_h} h_{\mathcal{K}}$ , where  $h_{\mathcal{K}} = \text{diam}(\mathcal{K})$ . The mesh conforms to the fault  $S$  as follows. We  
 805 construct a trapezoidal region inside  $\Omega$  with one side lying on the displacement-free part  $\Sigma$   
 806 of  $\partial\Omega$  and one side that agrees with the fault segment  $S$ . We then align the computa-  
 807 tional grid with  $S$  (see Fig. 4a).

808 We define  $F_I$  as the set of all interior sides. An interior side  $\gamma$  in  $F_I$  is characterized by  
 809 the existence of two adjacent elements  $K^+$  and  $K^-$  in  $\mathcal{T}_h$  such that  $\gamma = \partial K^+ \cap \partial K^-$ . For  
 810 clarity in presenting the DG formulation, we distinguish between the sides that belongs  
 811 to  $S$  from the others, which belong to  $\mathcal{F}_I$ .

812 Similarly, we label the sides of the elements that touch the boundary  $\partial\Omega$  according to  
 813 whether Dirichlet and Neumann conditions are imposed, grouping them into the families  
 814  $F_D$  and  $F_N$ , respectively:

815 
$$F_D = \{\gamma \mid \exists K \text{ such that } \gamma \subseteq \partial K \cap \partial\Omega_D\}$$
  
 816 
$$F_N = \{\gamma \mid \exists K \text{ such that } \gamma \subseteq \partial K \cap \partial\Omega_N\}$$

817 This definition assumes that the mesh conforms to the boundary decomposition of  $\partial\Omega$ ;  
 818 that is, every side  $\gamma$  belongs exclusively to either  $F_D$  or  $F_N$ .

819 Next, given an integer  $r \geq 1$  we define the finite-dimensional space of DG elements by:

$$820 \quad V_h^r = \left\{ \mathbf{v}_h \in L^2(\Omega) \mid \mathbf{v}_h^j|_K \in \mathcal{P}^r(K), j = 1, 2, \text{ for all } K \in \mathcal{T}_h \right\}$$

821 where  $\mathcal{P}^r(K)$  denotes the space of polynomials of total degree  $r$  defined on the element  $K$   
 822 and  $\mathbf{v}^j$  denotes the  $j$ -th component of the vector field  $\mathbf{v}$ . The approximate solution will be  
 823 sought in the space  $V_h^r$ , which is also the space of test functions.

824 **Trace operators**

825 To handle piecewise discontinuous functions, we use appropriate trace operators. Let  
 826  $\gamma \in \mathcal{F}_I$  be an interior side shared by two elements  $K^+$  and  $K^-$  of  $\mathcal{T}_h$ , with unit normal  
 827 vectors  $\mathbf{n}^+$  and  $\mathbf{n}^-$  pointing outward from  $K^+$  and  $K^-$ , respectively. On  $\gamma$ , we define  
 828 the average and jump operators for sufficiently regular vector-valued and tensor-valued  
 829 functions  $\mathbf{v}$  and  $\sigma$  as follows:

$$830 \quad \begin{aligned} \{\mathbf{v}\} &= \frac{1}{2}(\mathbf{v}^+ + \mathbf{v}^-), & \{\sigma\} &= \frac{1}{2}(\sigma^+ + \sigma^-) \\ \llbracket \mathbf{v} \rrbracket &= \mathbf{v}^+ \otimes \mathbf{n}^+ + \mathbf{v}^- \otimes \mathbf{n}^-, & \llbracket \sigma \rrbracket &= \sigma^+ \mathbf{n}^+ + \sigma^- \mathbf{n}^- \end{aligned} \tag{4.1}$$

831 where  $\mathbf{v} \otimes \mathbf{n} = \frac{1}{2}(\mathbf{v}\mathbf{n}^T + \mathbf{n}\mathbf{v}^T)$ .

832 The jump operator, defined using normal unit vectors, transforms a vector-valued func-  
 833 tion into a tensor-valued function and vice versa. This approach is preferable in numerical  
 834 schemes compared to the common definition  $\llbracket \mathbf{v} \rrbracket = \mathbf{v}^+ - \mathbf{v}^-$ , as it uses a sum instead  
 835 of a difference, leveraging its commutative property. This ensures that the operator is  
 836 independent of the element numbering ( $K^+$  and  $K^-$ ) during implementation. For edges  
 837  $\gamma$  on the boundary of the domain, i.e.,  $\gamma \in \mathcal{F}_D \cup \mathcal{F}_N$ , we set:

$$838 \quad \begin{aligned} \{\mathbf{v}\} &= \mathbf{v}^+, & \llbracket \mathbf{v} \rrbracket &= \mathbf{v}^+ \otimes \mathbf{n} \\ \{\sigma\} &= \sigma^+, & \llbracket \sigma \rrbracket &= \sigma^+ \mathbf{n} \end{aligned}$$

839 **Discontinuous Galerkin formulation**

840 In this section, we assume that the solution of (2.5) is sufficiently regular so as to jus-  
 841 tify integration by parts. Obtaining the weak formulation in the discontinuous Galerkin  
 842 form is possible, in principle, even for solutions and test functions belonging to  $H^1(\Omega)$ ,  
 843 provided that the traces of the gradient on the boundary of the elements are considered  
 844 in appropriate distribution spaces. However, to achieve global a priori error estimates  
 845 in the energy norm, higher regularity of the solution, such as assuming the solution in  
 846  $H^2(\Omega)$ , is needed [23,24], similarly to what happens in classical finite element methods.  
 847 By construction, both the approximate solution and the test function belong to the space  
 848  $V_h^r$  and hence have the required regularity.

849 To derive a variational formulation for the DG approximate solution, we begin by mul-  
 850 tiplying the first equation in (2.5) by a test function  $\mathbf{v} \in V_h^r$ . For notational convenience,  
 851 we extend  $\mathbf{u}$  and  $\mathbf{v}$  by zero to  $\overline{\Omega}^c$ , so that on  $\partial\Omega$  the jump of  $\mathbf{u}$  and  $\mathbf{v}$  agrees with their trace  
 852 value. We then integrate over a generic element  $K \in \mathcal{T}_h$  and apply integration by parts.  
 853 By summing over all elements  $K \in \mathcal{T}_h$ , we obtain:

$$854 \quad \sum_{K \in \mathcal{T}_h} \int_K \mathbb{C} \widehat{\nabla} \mathbf{u} : \widehat{\nabla} \mathbf{v} \, dx = \sum_{K \in \mathcal{T}_h} \int_{\partial K} (\mathbb{C} \widehat{\nabla} \mathbf{u} \mathbf{n}) \cdot \mathbf{v} \, dx. \tag{4.2}$$

We note that on the right-hand side of the identity above, the integrals over the sides of triangles in the partition are computed twice for triangles sharing a common side, once with the outward normal vector  $\mathbf{n}^+$  and once with  $\mathbf{n}^-$ .

Since  $\mathbf{u}$  solves (2.5), the traction is zero on all sides in  $\mathcal{F}_N$ , so that we can rewrite (4.2) as follows:

$$\sum_{K \in \mathcal{T}_h} \int_{\partial K} (\mathbb{C}\widehat{\nabla}\mathbf{u}) \cdot \mathbf{v} \, dx = \sum_{\gamma \in \mathcal{F}_I \cup S} \int_{\gamma} [(\mathbb{C}\widehat{\nabla}\mathbf{u})^+ \mathbf{n}^+ \cdot \mathbf{v}^+ + (\mathbb{C}\widehat{\nabla}\mathbf{u})^- \mathbf{n}^- \cdot \mathbf{v}^-] \, d\sigma(\mathbf{x}) + \sum_{\gamma \in \mathcal{F}_D} \int_{\gamma} (\mathbb{C}\widehat{\nabla}\mathbf{u}) \cdot \mathbf{v} \, d\sigma(\mathbf{x}),$$

Next, from the definitions of the average and jump operators given in (4.1) we have that

$$\begin{aligned} & \sum_{\gamma \in \mathcal{F}_I \cup S} \int_{\gamma} [(\mathbb{C}\widehat{\nabla}\mathbf{u})^+ \mathbf{n}^+ \cdot \mathbf{v}^+ + (\mathbb{C}\widehat{\nabla}\mathbf{u})^- \mathbf{n}^- \cdot \mathbf{v}^-] \, d\sigma(\mathbf{x}) + \sum_{\gamma \in \mathcal{F}_D} \int_{\gamma} (\mathbb{C}\widehat{\nabla}\mathbf{u}) \cdot \mathbf{v} \, d\sigma(\mathbf{x}) \\ &= \sum_{\gamma \in \mathcal{F}_I \cup \mathcal{F}_D \cup S} \int_{\gamma} \{\mathbb{C}\widehat{\nabla}\mathbf{u}\} : \llbracket \mathbf{v} \rrbracket \, d\sigma(\mathbf{x}) + \sum_{\gamma \in \mathcal{F}_I \cup S} \int_{\gamma} \llbracket \mathbb{C}\widehat{\nabla}\mathbf{u} \rrbracket \cdot \{\mathbf{v}\} \, d\sigma(\mathbf{x}). \end{aligned} \tag{4.3}$$

The second integral term on the right-hand side vanishes as  $\llbracket \mathbb{C}\widehat{\nabla}\mathbf{u} \rrbracket = 0$  on every interior side of the partition and across  $S$ , again using that  $\mathbf{u}$  is a variational solution of (2.5). The first integral term on the right-hand side does not vanish in general, because the test functions in  $V_h^r$  may jump across the sides of the partition. Since the bilinear form on the left-hand side of (4.2) is symmetric, for numerical accuracy it is important to preserve symmetry after integration by parts. To this end, using that the jump  $\llbracket \mathbf{u} \rrbracket = 0$  on  $\mathcal{F}_I \cup \mathcal{F}_D$ ,  $\llbracket \mathbf{u} \rrbracket = \mathbf{g}$  on  $S$ , and inserting (4.3) for the right-hand side of (4.2), we obtain the following variational formulation, which must be satisfied by the DG approximate solution:

$$\begin{aligned} & \sum_{K \in \mathcal{T}_h} \int_K \mathbb{C}\widehat{\nabla}\mathbf{u} : \widehat{\nabla}\mathbf{v} \, dx - \sum_{\gamma \in \mathcal{F}_I \cup \mathcal{F}_D \cup S} \int_{\gamma} \{\mathbb{C}\widehat{\nabla}\mathbf{u}\} : \llbracket \mathbf{v} \rrbracket \, d\sigma(\mathbf{x}) - \sum_{\gamma \in \mathcal{F}_I \cup \mathcal{F}_D \cup S} \int_{\gamma} \{\mathbb{C}\widehat{\nabla}\mathbf{v}\} : \llbracket \mathbf{u} \rrbracket \, d\sigma(\mathbf{x}) \\ &= - \sum_{\gamma \in S} \int_{\gamma} \mathbf{g} \otimes \mathbf{n}^+ : \{\mathbb{C}\widehat{\nabla}\mathbf{v}\} \, d\sigma(\mathbf{x}) \end{aligned} \tag{4.4}$$

It has been shown in [1,2] that adding a penalization of jumps in the form

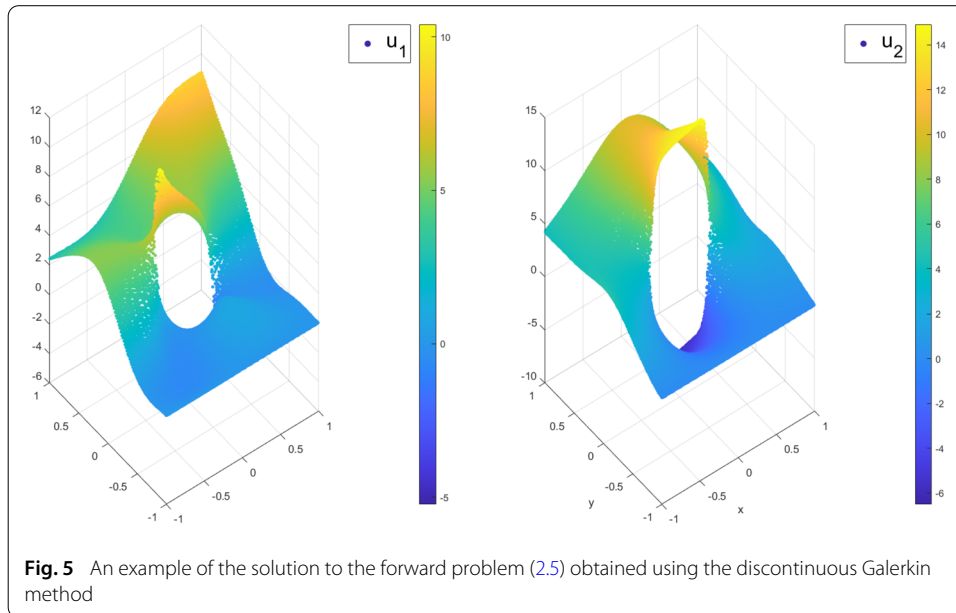
$$\int_{\gamma} \eta \llbracket \mathbf{u} \rrbracket : \llbracket \mathbf{v} \rrbracket \, d\sigma(\mathbf{x})$$

ensures the stability of the numerical method while preserving symmetry. It is crucial to choose the penalization parameter appropriately. We define  $\eta \in L^1(\mathcal{F}_I \cup \mathcal{F}_D \cup S)$  as follows:

$$\eta_{\gamma} = \beta \mathfrak{C} \frac{r^2}{h}, \quad \forall \gamma \in \mathcal{F}_I \cup \mathcal{F}_D \cup S,$$

where  $\beta$  is a positive constant,  $h$  is the mesh size,  $r$  is the polynomial degree, and  $\mathfrak{C}(\mathbf{x}) := (\sum_{i,j,h,k} |\mathbb{C}_{ijhk}(\mathbf{x})|^2)^{1/2}$  is the discrete 2-matrix norm. As the mesh is refined, specifically as  $h \rightarrow 0$ , the parameter  $\eta$  increases, thereby providing greater stabilization. The penalized DG variational formulation is finally given by:

$$\begin{aligned} & \sum_{K \in \mathcal{T}_h} \int_K \mathbb{C}\widehat{\nabla}\mathbf{u} : \widehat{\nabla}\mathbf{v} \, dx - \sum_{\gamma \in \mathcal{F}_I \cup \mathcal{F}_D \cup S} \int_{\gamma} \{\mathbb{C}\widehat{\nabla}\mathbf{u}\} : \llbracket \mathbf{v} \rrbracket \, d\sigma(\mathbf{x}) \\ & - \sum_{\gamma \in \mathcal{F}_I \cup \mathcal{F}_D \cup S} \int_{\gamma} \{\mathbb{C}\widehat{\nabla}\mathbf{v}\} : \llbracket \mathbf{u} \rrbracket \, d\sigma(\mathbf{x}) + \sum_{\gamma \in \mathcal{F}_I \cup \mathcal{F}_D \cup S} \int_{\gamma} \eta \llbracket \mathbf{u} \rrbracket : \llbracket \mathbf{v} \rrbracket \, d\sigma(\mathbf{x}) \\ &= - \sum_{\gamma \in S} \int_{\gamma} \mathbf{g} \otimes \mathbf{n}^+ : \{\mathbb{C}\widehat{\nabla}\mathbf{v}\} \, d\sigma(\mathbf{x}) + \sum_{\gamma \in S} \int_{\gamma} \eta \mathbf{g} \otimes \mathbf{n}^+ : \llbracket \mathbf{v} \rrbracket \, d\sigma(\mathbf{x}). \end{aligned} \tag{4.5}$$



885 Then the DG approximate solution  $u_h \in V_h^r$  of the forward problem (2.5) must satisfy  
 886 (4.5) for all  $v \in V_h^r$ , see [1–3, 23, 24]. We use a similar penalized formulation to compute  
 887 the DG solution  $w_h \in V_h^r$  of the adjoint problem (3.38). The numerical implementation  
 888 then follows the standard approach for finite elements methods.

889 In Fig. 5, we plot an example of the numerical solution for the forward problem (2.5),  
 890 obtained by using linear elements, that is, polynomials of degree 1 on each element  $K$ ,  
 891 and setting the mesh size  $h = 0.01$ . We consider the case of a horizontal dislocation with  
 892 vertices at  $(-0.4, 0)$  and  $(0.4, 0)$  and a slip field vanishing at the endpoint of the dislocation  
 893 segment given by

$$894 \mathbf{g}(s) = \left( 10 \left( - \left( \frac{100}{39} \right)^{12} s^{12} + 1 \right) \chi_{(-\frac{39}{100}, \frac{39}{100})}(s), 20 \left( - \left( \frac{100}{39} \right)^{12} s^{12} + 1 \right) \chi_{(-\frac{39}{100}, \frac{39}{100})}(s) \right),$$

895 (4.6)

#### 896 4.2 Reconstruction algorithm

897 For the reconstruction algorithm, we adopt the gradient descent approach introduced in  
 898 [9]. Below, we briefly recall the method as it applies to our problem.

899 To highlight the dependence of the shape derivative on the map  $\mathcal{U} \in W^{1,\infty}(\Omega)$ , identified  
 900 with a vector field on  $\mathbb{R}^2$ , that encodes the infinitesimal movement of the fault (see (3.2)),  
 901 in this section we will use the notation

$$902 \frac{d\mathcal{J}}{d\tau} \Big|_{\tau=0} = \langle D\mathcal{J}(S, \mathbf{g}), \mathcal{U} \rangle,$$

903 where  $D\mathcal{J}(S, \mathbf{g})$  represents the gradient. Furthermore, in all simulations we will assume  
 904 the slip field  $\mathbf{g}$  is known at the dislocation, focusing solely on reconstructing the dislocation  
 905 line. As we have already mentioned, if  $S$  can be reconstructed, the reconstruction of  $\mathbf{g}$  is  
 906 conceptually simpler as this part of the inverse problem is linear. In what follows hence,  
 907 we will focus on presenting the descent algorithm for the reconstruction of  $S$  given  $\mathbf{g}$ .

908 Consequently, for notational convenience we simply write

$$909 \quad \frac{d\mathcal{J}}{d\tau} \Big|_{\tau=0} = \langle D\mathcal{J}(S), \mathcal{U} \rangle.$$

910 We also use  $(\cdot, \cdot)$  to denote the  $L^2$ -inner product.

911 We also continue to specialize to the case that the dislocation line  $S$  is a straight segment,  
912 so it is uniquely determined by its two vertices  $\mathbf{P}_l \in \mathbb{R}^2, l = 1, 2$ .

913 A key step in the descent algorithm is the computation of the descent direction at each  
914 step. Let  $X \subset W^{1,\infty}(\Omega, \mathbb{R}^2)$  be a suitable subspace. Then, at iteration level  $k \in \mathbb{N}$ , we solve  
915 the equation

$$916 \quad ((\boldsymbol{\theta}^k, \delta\boldsymbol{\theta})) + \langle D\mathcal{J}(S^k), \delta\boldsymbol{\theta} \rangle = 0 \tag{4.7}$$

917 for every  $\delta\boldsymbol{\theta} \in X$ , where  $\boldsymbol{\theta}^k \in X$  denotes the descent direction and  $S^k$  is the dislocation  
918 line computed at the  $k$ -th iteration. The subspace  $X$  is chosen so that  $S^k$  is a segment  
919 contained in  $\Omega$  for each  $k$ . For solving (4.7), we discretize the problem and employ the  
920 idea already contained in [9]. That is, given that the dislocation line is uniquely defined by  
921 its vertices, we compute the descent direction for each vertex individually before updating  
922 the partition at each iteration  $k$ .

923 Specifically, we recall that we have two meshes. A coarse mesh used for the measure-  
924 ments and a fine mesh used for the DG approximation. The vertex of the dislocation  
925 segment is assumed to be on both meshes. At iteration level  $k$ , for each vertex  $\mathbf{P}_l^k, l = 1, 2$ ,  
926 of  $S^k$ , we calculate the gradient of the functional  $\mathcal{J}$  with respect to the position of the  
927 vertex  $\mathbf{P}_l^k$  as follows. We select two maps  $\mathcal{U}_{l,1}^k, \mathcal{U}_{l,2}^k \in W^{1,\infty}(\Omega, \mathbb{R}^2)$  with the properties  
928 that:

- 929 (1)  $\mathcal{U}_{l,1}^k, \mathcal{U}_{l,2}^k$  have support strictly contained within  $\Omega$ .
- 930 (2)  $\mathcal{U}_{l,1}^k$  and  $\mathcal{U}_{l,2}^k$  are piecewise linear along the sides of the (coarse) partition and satisfy

$$931 \quad \mathcal{U}_{l,1}^k(\mathbf{P}_j^k) = (\delta_{jl}, 0), \quad \mathcal{U}_{l,2}^k(\mathbf{P}_j^k) = (0, \delta_{jl}),$$

932 where  $\delta_{jl}$  denotes the Kronecker delta and  $\mathbf{P}_j^k$  denotes any vertex of the mesh.

933 Then, the gradient of  $\mathcal{J}$  with respect to the position of the vertex  $\mathbf{P}_l^k$  is given by:

$$934 \quad \left( \langle D\mathcal{J}(S^k), \mathcal{U}_{l,1}^k \rangle, \langle D\mathcal{J}(S^k), \mathcal{U}_{l,2}^k \rangle \right),$$

935 and hence the steepest descent at the  $k$ -th iteration is represented by the vector

$$936 \quad \boldsymbol{\theta}_{l,j}^k = - \left( \langle D\mathcal{J}(S^k), \mathcal{U}_{l,1}^k \rangle, \langle D\mathcal{J}(S^k), \mathcal{U}_{l,2}^k \rangle \right), \tag{4.8}$$

937 For the DG approximation, we define the maps  $\mathcal{U}_{l,1}^k$  and  $\mathcal{U}_{l,2}^k$  as follows:

$$938 \quad \mathcal{U}_{l,1}^k = (\varphi_l^k, 0), \quad \mathcal{U}_{l,2}^k = (0, \varphi_l^k),$$

939 where  $\varphi_l^k$  is the hat function associated with the node  $\mathbf{P}_l^k$  of the coarse mesh (see, for  
940 example, Fig. 4b); that is,  $\varphi_l^k$  is piecewise linear and

$$941 \quad \varphi_l^k(\mathbf{P}_j^k) = \delta_{jl}.$$

942 We then stop the algorithm when a desired tolerance is reached or a maximum number  
943 of iterations have occurred as customary. Below is a pseudocode for the reconstruction  
944 algorithm as implemented in MATLAB<sup>®</sup> for a specific set of parameters.

---

**Algorithm 1** Reconstruction Algorithm
 

---

```

1: Parameters:  $maxIter = 5000$ ,  $tol = 1 \times 10^{-7}$ ,  $\alpha = 1 \times 10^{-6}$ ,  $nIter = 150$ 
2: Initialize geometry and mesh
3: for  $k = 1$  to  $maxIter$  do
4:   Solve the forward problem (2.5)
5:   Compute gradient of the solution.
6:   Extract boundary data for adjoint problem
7:   Solve the adjoint problem (3.38)
8:   Compute gradient of the adjoint solution.
9:   Calculate shape derivatives using  $\mathcal{U}_1^k$  and  $\mathcal{U}_2^k$ .
10:  Update the vertices of the dislocation, using (4.8), i.e.,  $\mathbf{P}_l^{k+1} = \mathbf{P}_l^k - \alpha \theta_l^k$ .
11:  if  $k > nIter$  and  $\max(\theta_l^k) < tol$  then
12:    break (Convergence reached)
13:  end if
14:  Update geometry and mesh.
15: end for

```

---

#### 945 4.2.1 Numerical tests

946 All the numerical simulations presented in this section have been performed in  
 947 MATLAB<sup>®</sup>. As already mentioned, the computational domain is a square  $\Omega = [-1, 1] \times$   
 948  $[-1, 1]$ , with homogeneous Dirichlet boundary conditions on  $y = -1$ , modeling the buried  
 949 part of the boundary, and homogeneous Neumann boundary conditions on the other three  
 950 sides, modeling the exposed part of the boundary at the Earth's surface (see Fig. 3).

951 We include noise to the data to model measurement errors. Specifically, for a noiseless  
 952 boundary measurement  $\mathbf{u}_m \in H^{1/2}(\partial\Omega)$ , the noisy data  $\hat{\mathbf{u}}_m$  is generated by adding uniform  
 953 noise to  $\mathbf{u}_m$  as follows:

$$954 \quad \hat{\mathbf{u}}_m(\mathbf{x}) = \mathbf{u}_m(\mathbf{x}) + \varepsilon \|\mathbf{u}_m\|_{L^2(\partial\Omega)}.$$

955 where  $\varepsilon$  is a uniform random variable drawn from the interval  $(-a, a)$ , with  $a > 0$  deter-  
 956 mined based on the desired noise level (unless specified otherwise, we set  $a = 0.0007$ ). In  
 957 the numerical implementation, the noise is added pointwise to each node of the coarse  
 958 mesh used for the measurements. To quantify the noise level, we compute the relative  $L^2$   
 959 error:

$$960 \quad \frac{\|\hat{\mathbf{u}}_m - \mathbf{u}_m\|_{L^2(\partial\Omega)}^2}{\|\mathbf{u}_m\|_{L^2(\partial\Omega)}^2}.$$

961 We include this error for each of the numerical tests in the corresponding figure below.

962 We perform simulations both in the case of a slip field  $\mathbf{g} \in H_{00}^{\frac{1}{2}}(S)$ , for which the  
 963 variational formulation of the forward problem and the shape derivative is rigorously  
 964 justified, as well as in the case of constant slip field  $\mathbf{g}$ , a configuration often used in  
 965 seismology. For the constant slip field, we study the case of a highly anisotropic oblique  
 966 slip, setting:

$$967 \quad \mathbf{g} = (-10, 20).$$

968 The presence of singularities in the elastic displacement at the tips of the dislocation aides  
 969 in the reconstruction.

970 For the case of a slip vanishing at the endpoint of the dislocation segment, we choose a  
 971 slip that vanishes to high order, which makes the reconstruction more difficult:

$$g(s) = \left( -10 \left( -\left(\frac{100}{39}\right)^{12} s^{12} + 1 \right) \chi_{(-\frac{39}{100}, \frac{39}{100})}(s), 20 \left( -\left(\frac{100}{39}\right)^{12} s^{12} + 1 \right) \chi_{(-\frac{39}{100}, \frac{39}{100})}(s) \right), \tag{4.9}$$

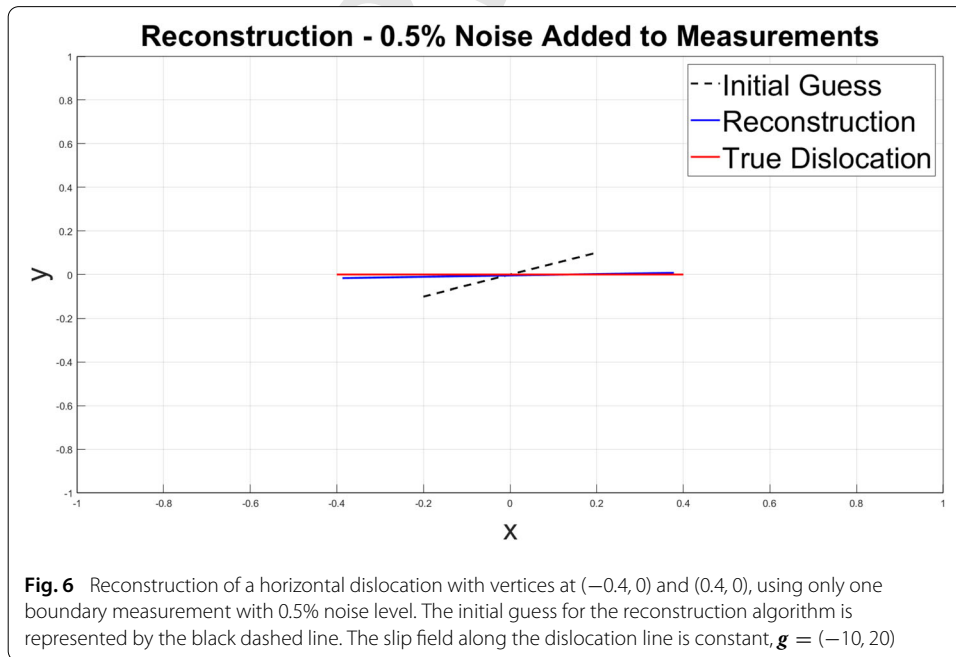
where  $\chi_{(-\frac{39}{100}, \frac{39}{100})}(s)$  is the characteristic function of the interval  $[-39/100, 39/100]$ , and the scalar  $s$  parameterizes the segment. Both cases are designed to test the limitation of the algorithm.

Similarly, the regularization parameter  $\alpha$  used for updating the dislocation vertices is chosen sufficiently small, but nonzero,  $\alpha = 10^{-6}$ . Finally, the elastic coefficients are taken constant to simplify the expression of the shape derivative and to improve stability. For simplicity, we set the Lamé coefficients  $\lambda = \mu = 1$ .

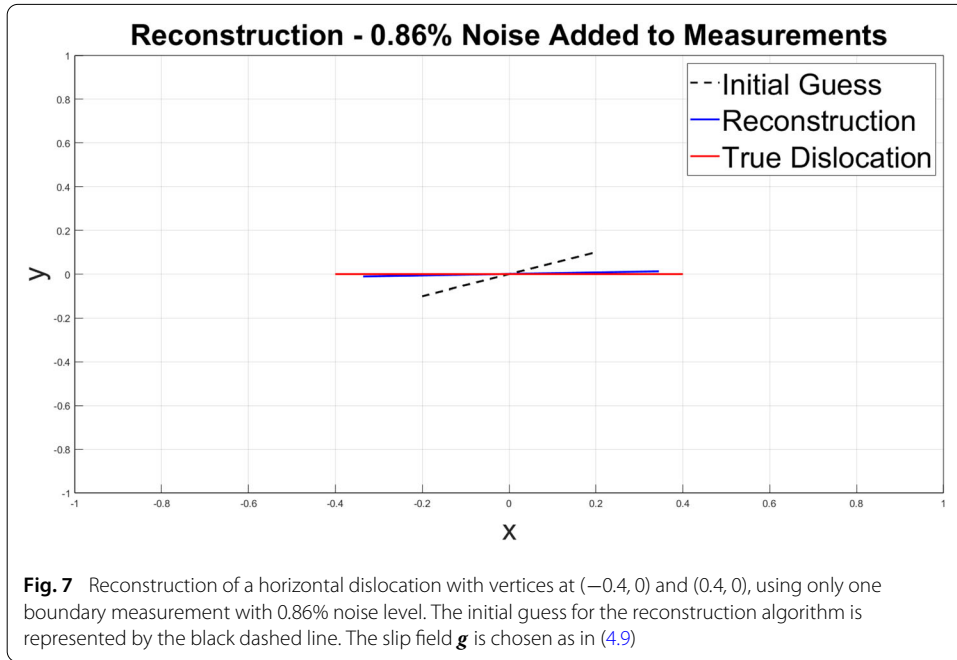
For most of the numerical tests, we measure the displacement on the entire exposed portion of  $\partial\Omega$ , the top and the two lateral sides of the square  $\Omega$ . One measurement is enough in this case to reconstruct the dislocation line  $S$ . For comparison, we include a test for which the displacement is measured only on the top side of  $\Omega$  (see Fig. 8 and Test 5). As expected, the reconstruction with one measurement is poor, and two measurements are needed in this case.

We include the results for the following numerical tests:

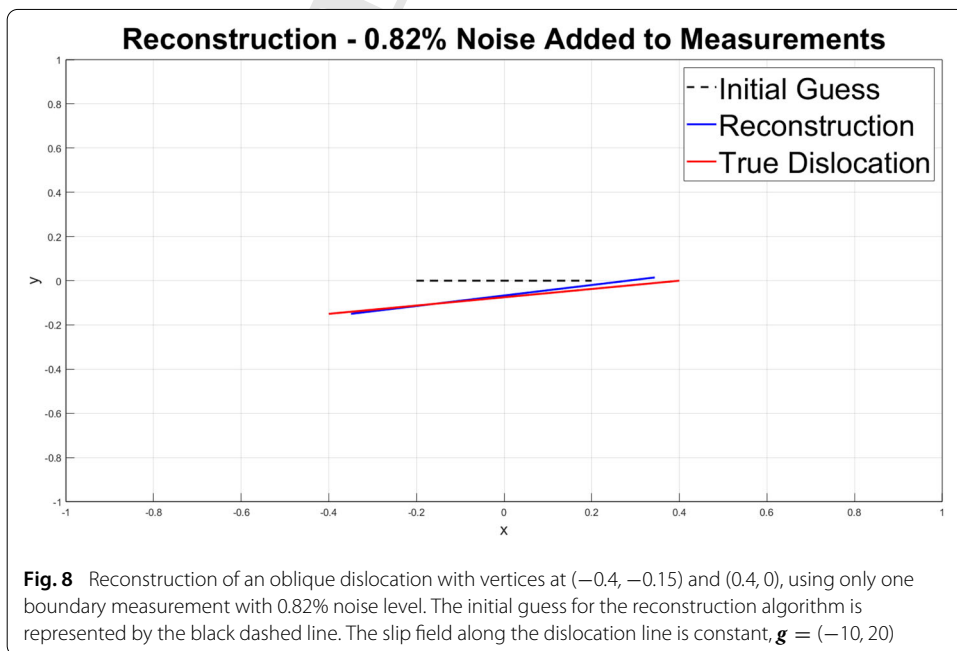
**Test 1: Horizontal dislocation with constant slip field  $g$  (Fig. 6).**



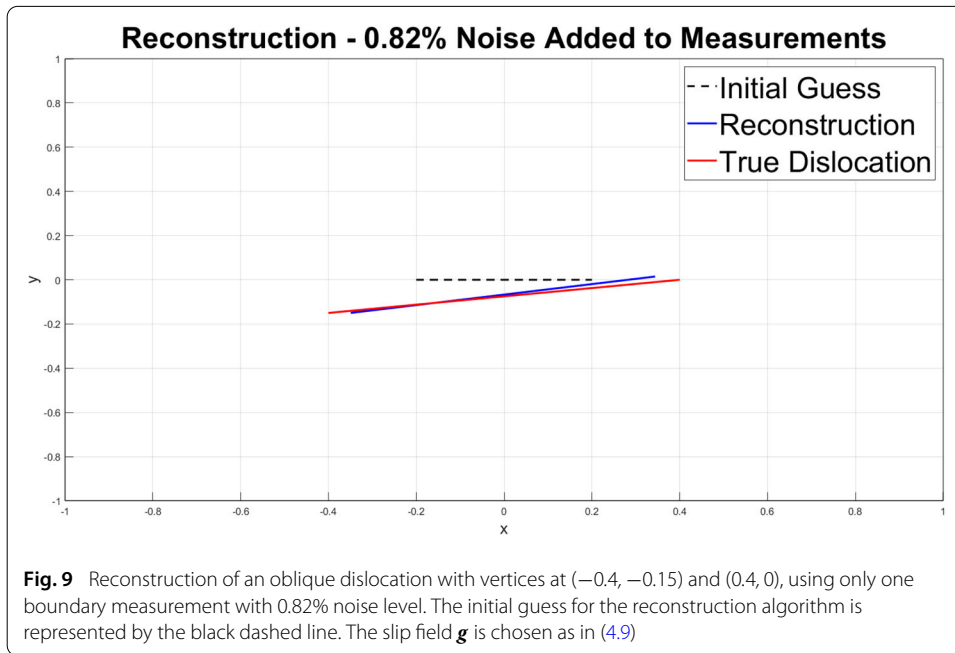
990 **Test 2: Horizontal dislocation with slip field  $g$  vanishing at the endpoints (Fig. 7)**



991 **Test 3: Oblique dislocation with constant slip field  $g$  (Fig. 8)**

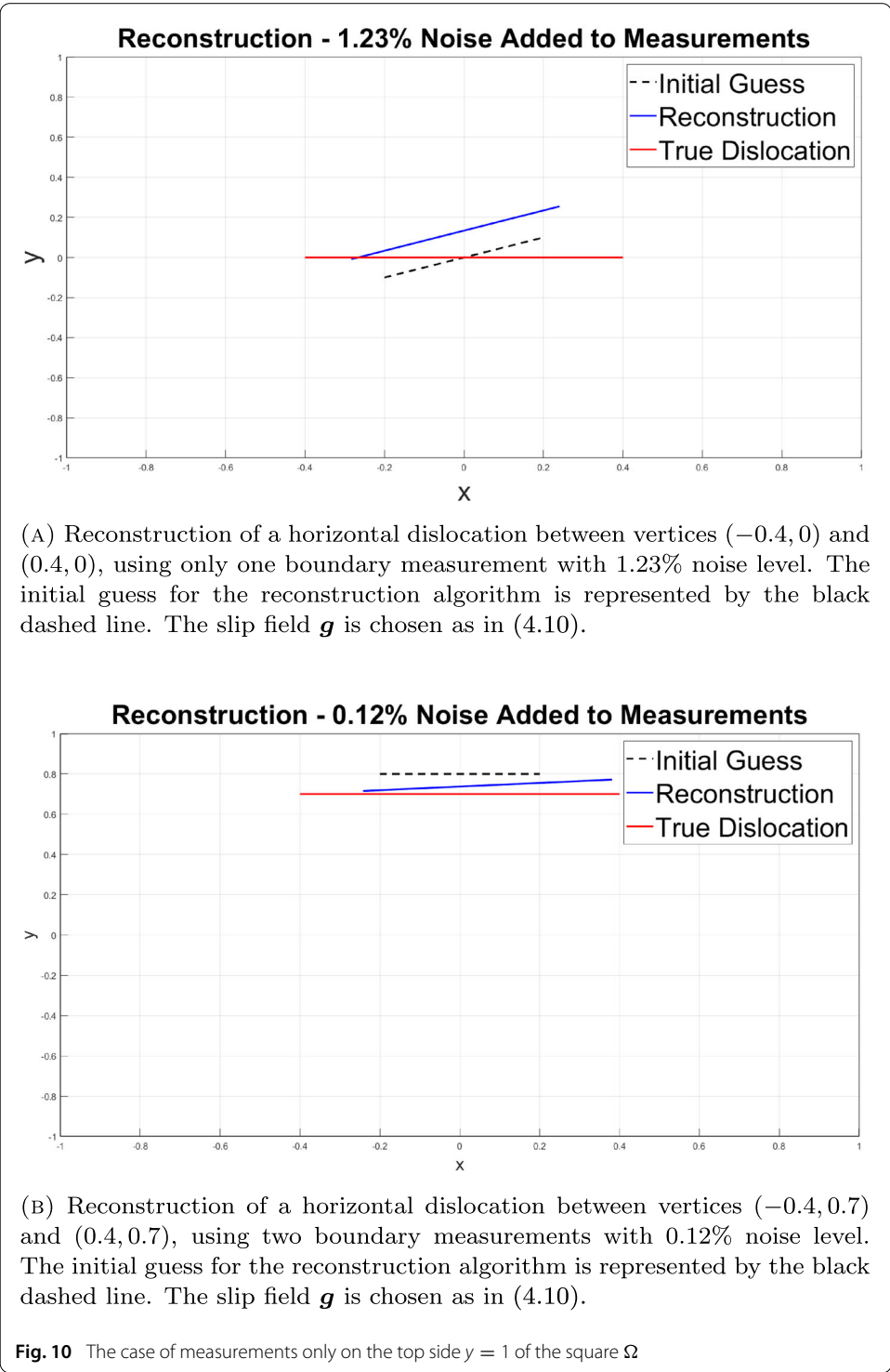


992 **Test 4: Oblique dislocation with slip field  $g$  vanishing at the endpoints (Fig. 9)**



993 **Test 5: Horizontal dislocation with slip field  $g$  vanishing at the endpoints and**  
 994 **measurements only on one side (Fig. 10).** In this numerical test, we consider the case  
 995 where measurements can only be collected on one side, specifically along the side given  
 996 by the points  $\{y = 1\}$ . As expected, in this case, the reconstructions are less accurate. In  
 997 particular, when assuming knowledge of only one boundary displacement measurement,  
 998 the reconstructions are of poor quality (see Fig. 10a). However, when more measurements  
 999 are available (still on the same side), the situation gradually improves (see Fig. 10b for the  
 1000 case of two measurements), even if the results are still not satisfactory. In this latter case,  
 1001 to generate the second measurement, we use the slip field  $g$  defined by the following data

$$\begin{aligned}
 \mathbf{g}(s) = & \left( 60 \left( -\left(\frac{1000}{395}\right)^{10} s^{10} + 1 \right) \chi_{\left(-\frac{395}{1000}, \frac{395}{1000}\right)}(s), \right. \\
 & \left. -10 \left( -\left(\frac{1000}{395}\right)^{10} s^{10} + 1 \right) \chi_{\left(-\frac{395}{1000}, \frac{395}{1000}\right)}(s) \right), \tag{4.10}
 \end{aligned}$$



### Acknowledgements

1005 The authors thank Paola Antonietti for useful discussion and for providing a MATLAB<sup>®</sup> package to implement the DG  
 1006 method. A. Mazzucato was partially supported by the US National Science Foundation Grants DMS-1909103,  
 1007 DMS-2206453, and thanks the hospitality of the Mathematics Program at New York University (NYUAD) and  
 1008 of the Mathematics Department at Milan University, where part of this work was conducted. This work was supported by  
 1009 a grant from the Simons Foundation (1036502, Mazzucato). Elena Beretta's research has been partially supported by  
 1010 NYUAD Science Program Project Fund AD364. A. Lee was also partially supported by the US National Science Foundation  
 1011 Grants DMS-1909103 and DMS-2206453. A. Aspri is member of the group GNAMPA (Gruppo Nazionale per l'Analisi  
 1012 Matematica, la Probabilità e le loro Applicazioni) of INdAM (Istituto Nazionale di Alta Matematica).

### Data availability

1013 All the data used in this work are synthetic data generated by an algorithm coded in MATLAB<sup>®</sup>. A description of the  
 1014 algorithm is included in the body of the manuscript. Output of the numerical scheme can be made available upon  
 1015 request.  
 1016

### Author details

1017 <sup>1</sup>Department of Mathematics "Federigo Enriques", University of Milan, Via Saldini 50, 20133 Milan, Italy, <sup>2</sup>Mathematics  
 1018 Program, Division of Science, New York University Abu Dhabi, PO Box 129188 Saadiyat Island, Abu Dhabi, UAE,  
 1019 <sup>3</sup>Mathematics Department, Penn State University, 107 McAllister Building, University Park, PA 16802, USA.

1020 Received: 3 October 2024 Accepted: 26 January 2025

### References

- 1021 1. Antonietti, P.F., Ayuso de Dios, B., Mazziere, I., Quarteroni, A.: Stability analysis of discontinuous Galerkin approximations  
 1022 to the elastodynamics problem. *J. Sci. Comput.* **68**(1), 143–170 (2016)
- 1023 2. Antonietti, P.F., Mazziere, I., Quarteroni, A., Rapetti, F.: Non-conforming high order approximations of the elastodynam-  
 1024 ics equation. *Comput. Methods Appl. Mech. Engrg.* **209**(212), 212–238 (2012)
- 1025 3. Arnold, D.N., Brezzi, F., Cockburn, B., Marini, L.D.: Unified analysis of discontinuous Galerkin methods for elliptic  
 1026 problems. *SIAM J. Numer. Anal.* **39**(5), 1749–1779 (2001)
- 1027 4. Aspri, A., Beretta, E., Mazzucato, A.L.: Dislocations in a layered elastic medium with applications to fault detection. *J.*  
 1028 *Eur. Math. Soc. (JEMS)* **25**(3), 1091–1112 (2023)
- 1029 5. Aspri, A., Beretta, E., De Hoop, M.V., Mazzucato, A.L.: Detection of dislocations in a 2D anisotropic elastic medium.  
 1030 *Rend. Mat. Appl.* **42**(3–4), 183–195 (2021)
- 1031 6. Aspri, A., Beretta, E., Mazzucato, A.L., De Hoop, M.V.: Analysis of a model of elastic dislocations in geophysics. *Arch.*  
 1032 *Ration. Mech. Anal.* **236**(1), 71–111 (2020)
- 1033 7. Beretta, E., Francini, E., Kim, E., Lee, J.-Y.: Algorithm for the determination of a linear crack in an elastic body from  
 1034 boundary measurements. *Inverse Probl.* **26**(8), 085015 (2010)
- 1035 8. Beretta, E., Francini, E., Vessella, S.: Determination of a linear crack in an elastic body from boundary measurements—  
 1036 Lipschitz stability. *SIAM J. Math. Anal.* **40**(3), 984–1002 (2008)
- 1037 9. Beretta, E., Micheletti, S., Perotto, S., Santacesaria, M.: Reconstruction of a piecewise constant conductivity on a  
 1038 polygonal partition via shape optimization in EIT. *J. Comput. Phys.* **353**, 264–280 (2018)
- 1039 10. Diao, H., Liu, H., Meng, Q.: Dislocations with corners in an elastic body with applications to fault detection. *arXiv*  
 1040 *e-prints*, page [arXiv:2309.09706](https://arxiv.org/abs/2309.09706), (2023)
- 1041 11. Eshelby, J.D.: Dislocation theory for geophysical applications. *Philos. Trans. R. Soc. A* **274**(1239), 331–338 (1973)
- 1042 12. Fichera, G.: The Italian contribution to the mathematical theory of elasticity. *Mecc. J. Ital. Assoc. Theoret. Appl. Mech.*  
 1043 **19**(4), 259–268 (1984)
- 1044 13. Guo, R., Lin, T., Lin, Y.: Recovering elastic inclusions by shape optimization methods with immersed finite elements. *J.*  
 1045 *Comput. Phys.* **404**, 109123 (2020)
- 1046 14. Harris, R.A.: Large earthquakes and creeping faults. *Rev. Geophys.* **55**(1), 169–198 (2017)
- 1047 15. Hsu, Y., Simons, M., Yu, S., Kuo, L., Chen, H.: A two-dimensional dislocation model for interseismic deformation of the  
 1048 Taiwan mountain belt. *Earth Planet. Sci. Lett.* **211**(3–4), 287–294 (2003)
- 1049 16. Ionescu, I.R., Volkov, D.: An inverse problem for the recovery of active faults from surface observations. *Inverse Probl.*  
 1050 **22**(6), 2103–2121 (2006)
- 1051 17. Ionescu, I.R., Volkov, D.: Detecting tangential dislocations on planar faults from traction free surface observations.  
 1052 *Inverse Probl.* **25**(1), 015012 (2009)
- 1053 18. Kaudur, S.B., Patil, M.J.: Shape optimization with immersed interface finite element method. *Internat. J. Numer.*  
 1054 *Methods Eng.* **123**(23), 5907–5936 (2022)
- 1055 19. Laurain, A.: Distributed and boundary expressions of first and second order shape derivatives in nonsmooth domains.  
 1056 *J. Math. Pures Appl.* **9**(134), 328–368 (2020)
- 1057 20. Mindlin, R.D.: Force at a point in the interior of a semi-infinite solid. In *Proceedings of The First Midwestern Conference*  
 1058 *on Solid Mechanics, April, 1953*, pp. 56–59. University of Illinois, The Engineering Experiment Station, Urbana, IL (1954)
- 1059 21. Morassi, A., Rosset, E.: Stable determination of cavities in elastic bodies. *Inverse Probl.* **20**(2), 453–480 (2004)
- 1060 22. Okada, Y.: Internal deformation due to shear and tensile fault in a half-space. *Bull. Seism. Log. Soc. Am.* **82**(2), 1018–  
 1061 1040 (1992)
- 1062 23. Rivière, B., Shaw, S., Wheeler, M.F., Whiteman, J.R.: Discontinuous Galerkin finite element methods for linear elasticity  
 1063 and quasistatic linear viscoelasticity. *Numer. Math.* **95**(2), 347–376 (2003)
- 1064 24. Schneider, R., Xu, Y., Zhou, A.: An analysis of discontinuous Galerkin methods for elliptic problems. *Adv. Comput.*  
 1065 *Math.* **25**(1–3), 259–286 (2006)
- 1066

- 1067 25. Segall, P.: *Earthquake and Volcano Deformation*. Princeton University Press (2010)
- 1068 26. Sokolowski, J., Zolésio, J.-P.: *Introduction to shape optimization*, volume 16 of *Springer Series in Computational Mathematics*. Springer-Verlag, Berlin (1992). Shape sensitivity analysis
- 1069
- 1070 27. Triki, F., Volkov, D.: Stability estimates for the fault inverse problem. *Inverse Probl.* **35**(7), 075007 (2019)
- 1071 28. van Zwieten, G., van Brummelen, E., van der Zee, K., Gutiérrez, M., Hanssen, R.: Discontinuities without discontinuity: the weakly-enforced slip method. *Comput. Methods Appl. Mech. Eng.* **271**, 144–166 (2014)
- 1072
- 1073 29. van Zwieten, G.J., Hanssen, R.F., Gutiérrez, M.A.: Overview of a range of solution methods for elastic dislocation problems in geophysics. *J. Geophys. Res. Solid Earth* **118**(4), 1721–1732 (2013)
- 1074
- 1075 30. Vergne, J., Cattin, R., Avouac, J.: On the use of dislocations to model interseismic strain and stress build-up at intracontinental thrust faults. *Geophys. J. Int.* **147**(1), 155–162 (2001)
- 1076
- 1077 31. Volkov, D.: Faults in elastic half space: direct and inverse problem. In *Imaging microstructures*, volume 494 of *Contemp. Math.*, pages 81–94. Amer. Math. Soc., Providence, RI (2009)
- 1078
- 1079 32. Volkov, D.: A stochastic algorithm for fault inverse problems in elastic half space with proof of convergence. *J. Comput. Math.* **40**(6), 957–978 (2022)
- 1080
- 1081 33. Volkov, D., Voisin, C., Ionescu, I.R.: Reconstruction of faults in elastic half space from surface measurements. *Inverse Probl.* **33**(5), 055018 (2017)
- 1082
- 1083 34. Volterra, V.: Sur l'équilibre des corps élastiques multiplement connexes. *Ann. Sci. École Norm. Sup.* **3**(24), 401–517 (1907)
- 1084
- 1085 35. Wang, K., Wells, R., Mazzotti, S., Hyndman, R., Sagiya, T.: A revised dislocation model of interseismic deformation of the cascadia subduction zone. *J. Geophys. Res. Solid Earth* **108** (2003)
- 1086

### 1087 **Publisher's Note**

1088 Springer Nature remains neutral with regard to jurisdictional claims in published maps and institutional affiliations.

Springer Nature or its licensor (e.g. a society or other partner) holds exclusive rights to this article under a publishing agreement with the author(s) or other rightsholder(s); author self-archiving of the accepted manuscript version of this article is solely governed by the terms of such publishing agreement and applicable law.